PHARMACIA

Pharmacia 72: 1–22
DOI 10.3897/pharmacia.72.e174188

Research Article

Anti-aging evaluation of transfersome and nanostructured lipid carrier gels containing *Curcuma longa* and *Glycyrrhiza glabra* extract on ultraviolet-B-irradiated rats

Oktavia Rahayu Adianingsih[1], Salma Latifani[1], Annisa Nur Fitriani[1], Anistasya Dwitama Wardani[1], Iffah Qurrotuain[1], Rachmad Tri Wahyudi[1], Azizah Maharani Putri Dewi[1], Jessica Aurellia Wahyu Dhinata[1], Gloria Angelica Rumabutar[1], Oktavia Eka Puspita[1], Bachtiar Rifai Pratita Ihsan[1], Wibi Riawan[2], Adeltrudis Adelsa Danimayostu[1], Valentina Yurina[1]

1 *Department of Pharmacy, Faculty of Medicine, Universitas Brawijaya, Malang, Indonesia*

2 *Department of Biomolecular Biochemistry, Faculty of Medicine, Universitas Brawijaya, Malang, Indonesia*

Corresponding author: Oktavia Rahayu Adianingsih (oktavia.rahayu@ub.ac.id)

Received 8 October 2025 ♦ **Accepted** 17 November 2025 ♦ **Published** 8 December 2025

Citation: Adianingsih OR, Latifani S, Fitriani AN, Wardani AD, Qurrotuain I, Wahyudi RT, Dewi AMP, Dhinata JAW, Rumabutar GA, Puspita OE, Ihsan BRP, Riawan W, Danimayostu AA, Yurina V (2025) Anti-aging evaluation of transfersome and nanostructured lipid carrier gels containing *Curcuma longa* and *Glycyrrhiza glabra* extract on ultraviolet-B-irradiated rats. Pharmacia 72: 1–22. https://doi.org/10.3897/pharmacia.72.e174188

Abstract

Skin aging is a multifactorial process influenced by intrinsic and extrinsic factors, particularly UV-B radiation. Natural ingredients such as *Curcuma longa* and *Glycyrrhiza glabra* show potential anti-aging effects. Transfersomes and nanostructured lipid carriers (NLCs) are delivery systems that have the potential to be developed for anti-aging applications. This study aimed to formulate transfersome and NLC systems loaded with turmeric and licorice extracts (TFS-CGE and NLC-CGE), evaluate their anti-aging effects through *in vitro* studies, and assess anti-photoaging effects in gel dosage form through an *in vivo* study. TFS-CGE and NLC-CGE formulations were developed using thin-layer hydration and hot homogenization methods, respectively, with optimization of lipid–surfactant and solid–liquid lipid ratios. The resulting nanoparticles were characterized for particle size, polydispersity index, zeta potential, morphology, entrapment efficiency, drug loading, and deformability. *In vitro* assays confirmed that both formulations exhibited antioxidant and anti-collagenase activities. Gel formulations of the optimized TFS-CGE and NLC-CGE were prepared for *in vivo* application. A UV-B-induced photoaging model in Wistar rats was used to evaluate anti-aging efficacy. After 3 weeks of topical treatment, TFS-CGE and NLC-CGE gels significantly improved skin elasticity, reduced epidermal thickness, and enhanced collagen density. Immunohistochemical analysis showed increased expression of elastin, TGF-β, and collagen types I, II, and III, along with reduced MMP-1 expression, indicating protective effects against UV-B-induced skin aging. These findings demonstrate that TFS-CGE and NLC-CGE gels are effective anti-aging formulations and help enhance skin delivery and bioactivity through a nanotechnology-based approach.

Keywords

aging, nanoparticle, NLC, transfersome, UV-B

Copyright *Adianingsih OR et al.* This is an open access article distributed under the terms of the Creative Commons Attribution License (CC-BY 4.0), which permits unrestricted use, distribution, and reproduction in any medium, provided the original author and source are credited.

PENSOFT

Introduction

Skin aging is a complex process involving intrinsic and extrinsic factors. Intrinsic factors include genetic, hormonal, and biochemical processes that cause irreversible degeneration of skin tissue, such as decreased dermis fibroblasts and skin tissue elasticity. The main extrinsic factor is exposure to UV radiation, which produces fine lines and hyperpigmentation on the skin. Skin that experiences photoaging demonstrates a significant decrease in the amount of collagen (Altay Benetti et al. 2023). Currently, many consumers tend to use cosmetic products made from natural ingredients. Natural compounds derived from plants are becoming popular because they are safer and act through different mechanisms of action on several signaling pathways for skin aging (Costa et al. 2022). Turmeric (*Curcuma longa*) and licorice root (*Glycyrrhiza glabra*) are two plants with anti-aging activity that have both been widely studied. Turmeric has strong antioxidant and anti-inflammatory activity (Benameur et al. 2021; Waghule et al. 2020). It can improve skin damage conditions due to UV radiation, such as erythema and skin wrinkles, and reduce epidermal thickening in mice irradiated with UV-B for 8 weeks (Zheng et al. 2020). Moreover, treatment with *Curcuma longa* extract significantly reduces tumor necrosis factor-α (TNF-α) and increases type-1 collagen expression in UV-B-irradiated mice skin, which demonstrates the anti-aging properties of turmeric (Threskeia et al. 2023). Previous research on the anti-aging activity of licorice has identified mechanisms such as inhibiting pigmentation (anti-tyrosinase), inhibiting oxidative stress (antioxidant), inhibiting aging due to UV radiation (anti-photoaging), and preventing degradation of collagen and the extracellular matrix of the dermis (anti-wrinkle) (Cerulli et al. 2022). Based on our previous network pharmacology study, a combination of both plants shows potential in targeting multiple pathways related to skin photoaging, with key bioactives such as curcumin, isoliquiritigenin, and demethoxycurcumin, warranting further experimental validation (Adianingsih et al. 2024).

However, the extract will not be effective if it is unable to penetrate the viable epidermis or deeper into the dermis. This can be overcome with a nanotechnology-based delivery system for active skin care ingredients. There are several types of nanodelivery systems, such as liposomes, transfersomes, niosomes, nanospheres, polymeric nanoparticles, nanostructured lipid carriers (NLCs), and solid lipid nanoparticles (SLNs), which are popularly used for cosmetic preparations (Kaul et al. 2018; Matei et al. 2021). Transfersomes are a modification of liposomes with high deformability, elasticity, and ultra-flexibility due to the addition of single-chain surfactant as an edge activator, thus reducing surface tension, which causes a decrease in the rigidity of the lipid bilayer membrane. Transfersomes are superior to liposomes because of their elastic properties; therefore, they are able to penetrate the dermis layer (Sguizzato et al. 2021). Several studies indicate that transfersomes are able to increase the penetration and delivery of anti-aging cosmeceutical active ingredients, including epigallocatechin gallate (Avadhani et al. 2017), n-acetylcysteine (Harmita et al. 2020), amniotic mesenchymal stem cell metabolite products (Ayunin et al. 2022), and tempranillo grape extract (Asensio-Regalado et al. 2022).

Nanostructured lipid carrier (NLC) is the second generation of lipid nanoparticles. It was developed to overcome the shortcomings of SLN, since it has a high drug loading capacity due to the presence of liquid lipids, thereby improving stability. NLC is prepared by mixing liquid and solid lipids with a recommended ratio of 70:30 to 99.9:0.1. An example of a product on the market that uses the NLC system is Cutanova-Cream Nanorepair Q10, which contains the active ingredient Q10 as an anti-aging agent (Kaul et al. 2018). The usage of NLC Q10 cream for 28 days showed a significant increase in skin hydration when compared with oil-in-water (O/W) type cream without NLC (only Q10) (Pardeike et al. 2010). NLC has been applied to develop cosmetic products with several anti-aging active ingredients, including coenzyme Q10, resveratrol, curcumin, and ellagic acid (Assali and Zaid 2022); basil (*Ocimum sanctum*) extract (Chaiyana et al. 2021); and rice bran extract (Manosroi et al. 2012).

This research aims to formulate gels containing *Curcuma longa* and *Glycyrrhiza glabra* extracts loaded into two types of nano-sized lipid-based delivery systems, transfersome (TFS-CGE) and NLC (NLC-CGE). The resulting formulas were evaluated based on their physical properties. *In vitro* tests were performed to assess antioxidant and anticollagenase activities, while *in vivo* experiments using UV-B-induced aging in rats were conducted to examine the effects of TFS-CGE and NLC-CGE gels on various skin aging parameters. This study may support the potential use of turmeric and licorice extract combination as more effective natural anti-aging agents through the use of nano-delivery systems.

Materials and methods

Plant extraction

The turmeric (*Curcuma longa*) and licorice (*Glycyrrhiza glabra*) powder and taxonomical identity were obtained from UPT Herbal Laboratory Balai Materia Medica, Batu, East Java, Indonesia (voucher no: 000.9.3/1832/102.20/2024 for turmeric and no: 000.9.3/1833/102.20/2024 for licorice). The extracts of turmeric and licorice were prepared by maceration using 96% ethanol, with a simplicial and solvent ratio of 1:10 for turmeric and 1:5 for licorice. The maceration was carried out for 24 hours with stirring for 30 minutes at 300 rpm using an overhead stirrer (RW 20 digital, IKA, Germany). It was followed by two remacerations, each with the same duration. All the filtrate was combined and then filtered through fine filter paper using a vacuum pump (Model DOA-P504-BN, GAST, USA) and was concentrated using a rotary evaporator (RV 10 basic, IKA, Germany) with a chiller (MC 350, Lauda, Germany) at 40 °C with a speed of 70 rpm under vacuum conditions (MZ 2C NT, Vacuumbrand, Germany). The ethanolic ex-

tract was dried using an oven (ED 53, Binder, Germany) at 40 °C for three days and then stored in a refrigerator at 4 °C (Vardhini et al. 2023).

Preparation of transfersome

Transfersome of *Curcuma longa* and *Glycyrrhiza glabra* (TFS-GCE) was prepared using thin-layer hydration, with modifications from previous research (Khatoon et al. 2019; Dudhipala et al. 2020). TFS was prepared using the formula shown in Table 1. Turmeric extract was dissolved in methanol and sonicated for 5 minutes using an ultrasonic device (M2800, Branson Ultrasonic, Emerson, Japan). Soy lecithin was dissolved in 10 mL of chloroform, and Tween 80 was dissolved in methanol. Phospholipid, surfactant, and turmeric extract were mixed and stirred until homogeneous (organic phase). The mixture was evaporated for 20 minutes at 60 °C with a speed of 25 rpm, gradually increasing 25 rpm every 2 minutes up to 250 rpm using a rotary evaporator under vacuum conditions. The thin layer was left for 2 hours while rotating at room temperature at 250 rpm for 120 minutes under vacuum conditions. Thereafter, the thin layer was hydrated with licorice extract solution in 50 mL PBS pH 7.4. The hydration process was performed at 100 rpm for 60 minutes at room temperature, followed by a 5-minute shaking period. TFS was left at room temperature for 2 hours, then sonicated for 60 minutes, and extruded using a 450 nm filter membrane for five cycles to reduce particle size. All TFS-CGE was stored in a refrigerator at 4 °C until further analysis. A blank transfersome formulation (base) was prepared following the same procedure, excluding the incorporation of licorice and turmeric extracts.

Table 1. Formulation of TFS-GCE.

Composition	FT1	FT2	FT3
Curcuma longa extract	0.25 g	0.25 g	0.25 g
Glycyrrhiza glabra extract	0.25 g	0.25 g	0.25 g
Soy lecithin	0.6375 g	0.6 g	0.5625 g
Tween 80	0.1125 g	0.15 g	0.1875 g
PBS pH 7.4	50 ml	50 ml	50 ml

Preparation of NLC

NLC of *Curcuma longa* and *Glycyrrhiza glabra* (NLC-CGE) was prepared using hot emulsification and ultrasonication, with modifications from previous research (Ahalwat and Bhatt 2022). NLC was formulated according to the composition presented in Table 2. In brief, solid and liquid lipids were heated at 80 °C. Separately, the aqueous phase was heated at the same temperature. After dissolving, *Curcuma longa* extract was added to the lipid phase with stirring at 500 rpm using a magnetic stirrer for 15 minutes at 80 °C. Then, 1 mL of the water phase was taken to dissolve the *Glycyrrhiza glabra* extract. To make a water-in-oil emulsion (primary emulsion), the water phase that had been added with *Glycyrrhiza glabra* extract was then added to the lipid phase by stirring at 1500 rpm using a magnetic stirrer for 15 minutes at 80 °C. The remaining surfactant was added and stirred at 2000 rpm for 2 hours using an overhead stirrer to make a secondary emulsion. The NLC formed was sonicated for 15 minutes at 60 °C using an ultrasonic device and cooled in an ice bath for 15 minutes at 2–4 °C. The NLC formed was then stored in a refrigerator at 2–4 °C. The NLC blank formulation was prepared using the same method as the active formulation but without the incorporation of extracts.

Table 2. Formulation of NLC-CGE.

Composition	FN1	FN2	FN3
Curcuma longa extract	0.25 g	0.25 g	0.25 g
Glycyrrhiza glabra extract	0.25 g	0.25 g	0.25 g
Stearic acid	3.15 g	2.8 g	2.45 g
Caprylic/capric triglyceride	0.35 g	0.7 g	1.05 g
Cremophor RH 40	1.5 g	1.5 g	1.5 g
Aquadest	50 ml	50 ml	50 ml

HPLC method validation for curcumin and glycyrrhizin determination

Chromatographic separation was performed using high-performance liquid chromatography (HPLC) (LC-2030C 3D Plus, Shimadzu, Japan) on a C18 column (4.6 mm × 150 mm, 5 µm). The mobile phase consisted of acetonitrile (Fisher Scientific, Fair Lawn, NJ, USA) and water (Ikapharmindo Putramas, Jakarta, Indonesia) that had been mixed with 3.3% glacial acetic acid (45:55) for curcumin determination and methanol: 0.4% phosphoric acid (68:32) for glycyrrhizin determination, both with isocratic elution at a flow rate of 1.0 mL/min. For curcumin analysis, the injection volume was 20 µL, with a column temperature of 30 °C and detection at a wavelength of 426 nm using a PDA detector. For glycyrrhizin analysis, the injection volume was 10 µL, with a column temperature of 35 °C and detection at a wavelength of 254 nm using a PDA detector.

A standard solution of 1000 ppm curcumin and glycyrrhizin (Tokyo Chemical Industry, Tokyo, Japan) was prepared by weighing 10 mg of the standard using an analytical balance, dissolving it in 10 mL of solvent, and sonicating for 5 minutes. The 1000 ppm solution was pipetted 5 mL and later diluted into a 50 mL volumetric flask to obtain a solution with a concentration of 100 ppm. For curcumin, a 100 ppm solution was further diluted into 1, 2, 3, 4, and 5 mL portions, each dissolved in 10 mL of solvent to obtain solutions with concentrations of 10, 20, 30, 40, and 50 ppm, respectively. For glycyrrhizin, a 100 ppm solution was further pipetted into 3, 4, 5, 6, and 7 mL portions, each dissolved in 10 mL of solvent to obtain solutions with concentrations of 30, 40, 50, 60, and 70 ppm, respectively.

The extract sample solution for method validation was prepared by weighing 50 mg of turmeric extract (for curcumin) or 105 mg of licorice extract (for glycyrrhizin) using an analytical balance and dissolving it in a 25 mL volumetric flask. The sample was sonicated for 10–15 minutes until homogeneous. Meanwhile, the sample solution for concentration determination was prepared by weighing

25 mg of turmeric extract (for curcumin) or 62.5 mg of licorice extract (for glycyrrhizin), dissolving it in a 10 mL volumetric flask, and sonicating for 10–15 minutes until homogeneous. The sonicated solution was then pipetted in 3 mL with a volumetric pipette and placed in a 10 mL volumetric flask.

Parameters used in validating analytical methods include selectivity, linearity, limit of detection (LOD), limit of quantification (LOQ), accuracy, and precision (United States Pharmacopoeia 36, 2017). The selectivity test was conducted by injecting a standard solution of 30 ppm curcumin or 50 ppm glycyrrhizin and 20 µL of the extract sample solution into the HPLC system. Selectivity was determined by evaluating the interference of other compounds in the turmeric or licorice extract and the mobile phase components. The linearity test was carried out by injecting standard solutions of curcumin at concentrations of 10, 20, 30, 40, and 50 ppm (for curcumin) or 30, 40, 50, 60, and 70 ppm (for glycyrrhizin) as much as 20 µL (for curcumin) or 10 µL (for glycyrrhizin) into the HPLC system. The area was observed, and the linear regression line equation was obtained from the data. LOD and LOQ values were determined by injecting standard solutions of curcumin or glycyrrhizin at the same concentration as the linearity. The peak was observed, and LOD and LOQ calculations were carried out according to the formula.

The accuracy and precision test for the addition method was carried out by preparing a curcumin standard solution or a glycyrrhizin standard solution of 1000 ppm. The turmeric or licorice extract sample solution was pipetted into three different 10 mL volumetric flasks (1 mL each) and then added to the standard solution at concentrations of 80, 100, and 120 µL (for curcumin) or 240, 300, and 360 µL (for glycyrrhizin). The solvent was added to the limit mark, obtaining three different concentration levels: 18, 20, and 22 ppm (for curcumin) or 54, 60, and 66 ppm (for glycyrrhizin). The volumetric flasks were replicated three times, resulting in a total of nine samples. Each sample was injected with volumes ranging from 20 µL (for curcumin) to 10 µL (for glycyrrhizin) into the HPLC system. The peak area was observed, and the resulting area data were entered into the linear regression line equation to calculate %recovery and %relative standard deviation (%RSD).

The curcumin content in turmeric extract samples and glycyrrhizin content in licorice extract samples were determined by injecting 20 µL (for curcumin) or 10 µL (for glycyrrhizin) of the prepared extract sample solution into the HPLC system. The peak area was observed, and the area data were entered into the linear regression line equation to quantify the levels of curcumin or glycyrrhizin in the extract samples.

Characterization of Transfersome and NLC

Physical characterization

Transfersomes and NLC were characterized for particle size, polydispersity index (PDI), and zeta potential using a Particle Size Analyzer (PSA) Microtrac® at the Faculty of Mathematics and Natural Science Laboratory, Yogyakarta State University. All the tests were performed in triplicate. The morphology of TFS and NLC was observed using Field-Emission Scanning Electron Microscopy (FESEM) FEI Quanta FEG 650 (US). Both samples were dried at room temperature and coated with platinum. Analysis was carried out at a magnification of 3000× to 5000×.

Drug entrapment efficiency and drug loading

Entrapment efficiency was prepared using the indirect method (Zhu et al. 2022). Two mL of transfersome was placed in a microtube and centrifuged at a speed of 14,500 rpm for 45 minutes at room temperature, while 1 mL of NLC was dissolved in 1 mL of methanol and centrifuged at a speed of 20,000 rpm for 45 minutes. The supernatant was taken, and the active substances (curcumin and glycyrrhizin) were measured using HPLC. Entrapment efficiency was calculated by Equation 1. The drug loading value in transfersome was calculated using Equation 2. Meanwhile, the drug loading value in NLC was calculated using Equation 3.

$$\text{Entrapment efficiency} = \frac{\text{total drug-free drug}}{\text{total drug}} \times 100\% \quad (1)$$

$$\text{Drug Loading} = \frac{\text{total drug} - \text{free drug}}{\text{total lipid} + \text{surfac tan } t + \text{total drug}} \times 100\% \quad (2)$$

$$\text{Drug loading} = \frac{\text{total drug} - \text{free drug}}{\text{total lipid} + \text{total drug}} \times 100\% \quad (3)$$

Deformability test

Deformability tests were performed for transfersomes to measure their deformability and elasticity properties. The deformability test was carried out by passing 5 mL of transfersome through a 100 nm filter membrane for 15 minutes at a certain pressure. Then, the size of the transfersome vesicles after extrusion was measured. The deformability index is determined by Equation 4 (Surini et al. 2018). Transfersome deformability can also be determined through percent deformability by comparing the vesicle sizes before and after extrusion (Dudhipala et al. 2020). Percent deformability is determined by Equation 5.

$$\text{Deformability index} = \text{total amount of transfersom passed} \times \left(\frac{\text{vesicle size after extrusion}}{\text{pore size of membrane}}\right)^2 \quad (4)$$

$$\text{Deformability}(\%) = \left(\frac{\text{vesicle size after extrusion}}{\text{vesicle size before extrusion}}\right) \times 100\% \quad (5)$$

In vitro anti-aging activity of transfersome and NLC through antioxidant and anti-collagenase tests

The antioxidant test was performed using the 2,2-diphenyl-1-picrylhydrazyl (DPPH) method. Sample preparation for the formulation and extracts was performed at various concentrations, involving the dissolution of the sample in methanol (Merck & Co., Darmstadt, Germany) and sonicating for 5 to 10 minutes. DPPH was prepared at a concentration of 30 ppm using the DPPH reagent (U6GJC-WA, TCI Chemical, Japan). Then, 1 mL of the sample was mixed with 3 mL of DPPH and incubated for 30 minutes. After incubation, measurements were taken using a UV–Vis spectrophotometer (UV-1800 240 V, Shimadzu, Japan) at a wavelength of 517 nm. The inhibition percentage was calculated by measuring the reduction in DPPH absorbance relative to the control (Adianingsih et al. 2024). The anti-collagenase test was performed according to the kit procedure using the Collagenase Activity Colorimetric Assay Kit (Sigma-Aldrich, MAK293, MO, USA). The sample preparation for the formulation was performed at an extract concentration of 80 ppm, based on the optimization results of the DPPH test, and added to the well at 10 µL. The sample was then mixed with the reagent according to the kit procedure and measured using a spectrophotometric multi-well plate reader at a wavelength of 345 nm for 14 minutes at 37 °C.

Preparation of transfersome and NLC-based gel for *in vivo* study

Five different gel formulations were prepared for the *in vivo* study. These included (1) a transfersome gel containing *Curcuma longa* and *Glycyrrhiza glabra* extracts (TFS-CGE gel), (2) an NLC gel containing the same extracts (NLC-CGE gel), (3) a blank transfersome gel without extracts (TFS base gel), (4) a blank NLC gel without extracts (NLC base), and (5) a gel containing the extracts without any nanocarriers (CGE gel). All gels were prepared by dispersing Carbopol 940 (3% w/v) into the respective formulation under continuous stirring at room temperature, followed by a 24-hour swelling period and neutralization with triethanolamine (TEA) to achieve the desired gel consistency.

Stability test of gels

The physical stability of the gels was evaluated over a 30-day storage period at 4 °C (Lin et al. 2024). The parameters assessed included pH, viscosity, and visual appearance. pH values were measured using a calibrated digital pH meter, while viscosity was determined using a viscometer (measured in cP). The visual appearance was evaluated macroscopically and rated on a three-point scale: +++ (good), ++ (average), and + (poor). Measurements were taken on day 0 and day 30.

Study design for an *in vivo* anti-aging study

Thirty-five male Wistar rats weighing 150–200 g were used in this study. All animal experimental procedures and protocols were approved by the Ethics Committee, Faculty of Medicine, Universitas Brawijaya, Indonesia (Number 155/EC/KEPK/06/2024). Rats were maintained under a standard environmental laboratory at 23 ± 2 °C, a humidity of 50 ± 10%, and a 12-hour light/dark cycle and were given free access to a standard diet and water *ad libitum*. After a week of acclimation, rats were randomly allocated to seven groups of five rats each (Table 3). Before treatment, the dorsal skin of rats (3×3 cm^2) was shaved to remove any hair with a mechanical shaver. Prior to epilation, the rats were anesthetized using 0.1% ketamine.

Table 3. Animal groups.

Group	Experimental procedure
Control	Normal and non-UVB irradiated group
UV-B	UV-B irradiated and non-treated group
UV-B + TFS-CGE gel	UV-B irradiated and treated with gel containing TFS *Curcuma longa* dan *Glycyrrhiza glabra* extract
UV-B + NLC-CGE gel	UV-B irradiated and treated with gel containing NLC *Curcuma longa* dan *Glycyrrhiza glabra* extract
UV-B + TFS base gel	UV-B irradiated and treated with gel containing TFS-base (without extracts)
UV-B + NLC base gel	UV-B irradiated and treated with gel containing NLC-base (without extracts)
UV-B + GCE gel	UV-B irradiated and treated with gel containing *Curcuma longa* dan *Glycyrrhiza glabra* extracts

Skin aging induction and treatment

A single UV-B lamp provided the UV-B light source (25 W; Exo Terra Reptile UVB200, Rolf C. Hagen Inc., CA, USA) with a wavelength of 290–320 nm and radiation intensity at a 10 cm distance of 0.225 mW/cm^2. The rats were exposed to UV-B three times weekly on alternate days at a distance of 10 cm from the light, and topical treatment was applied to the dorsal skin 5 minutes after exposure to UV-B. The UV-B dose increased weekly in one minimal erythema dose (MED; one MED is 135 mJ/cm^2) up to three MED, corresponding to exposure durations of 10 to 30 minutes. The MED value was determined by irradiating the rats with UV-B at various durations (5, 10, 15, 20, 30, and 60 minutes). The results found that irradiation with a duration of 10 minutes produced minimal erythema after 48 hours of exposure and calculated the MED (Chawla et al. 2021).

A pinch test was conducted to investigate the dorsal skin elasticity of the mice based on the method described by Tsukahara et al. (2005). The test was performed every last day of each week, five minutes after UV-B exposure. In detail, the midline of the dorsal skin of the mouse was lifted until its feet lightly touched the table, then the pinch was released while measuring the recovery time of the skin to its original state. After carbon dioxide (CO_2) euthanasia, dorsal rat skin samples (3 × 3 cm) were collected, fixed in 10% neutral buffer formalin (NBF) for 24–48 hours, and subsequently embedded in paraffin. The samples were then sectioned at a thickness of 5 μm and stained with hematoxylin and eosin (H&E), Masson's trichrome, and specific antibodies for immunohistochemical analysis.

Histopathological analysis

Hematoxylin–eosin (H&E) staining was performed at the Laboratory of Anatomy, while Masson's trichrome staining was conducted at the Laboratory of Pathological Anatomy, Faculty of Medicine, Universitas Brawijaya. In brief, the skin was fixed in 10% NBF, paraffin-embedded, tissue sectioned at 5 μm, deparaffinized, rehydrated, and stained with H&E or Masson's trichrome. H&E staining was used for histological observations of skin structure and epidermal thickness, whereas Masson's trichrome stain was used for the density of collagen fibers in the dermis (Zhu et al. 2022). Variables were analyzed at five random locations per slide using an Optilab microscope biology trinocular (Miconos, Yogyakarta, Indonesia) using 400× magnification. Each specimen was photographed under the Optilab Advance+ digital camera microscope (Miconos, Yogyakarta, Indonesia) with Optilab Viewer software. Epidermal thickness was measured using Optilab Viewer software, which had already been calibrated. Collagen fiber density was evaluated using the ImageJ 1.53e software (National Institutes of Health, Maryland, USA).

Immunohistochemistry

Immunohistochemical staining was performed following the protocol from the Diagnostic BioSystems PolyVue™ Plus Kit (PVP250D, Diagnostic BioSystems, Pleasanton, CA, USA). Skin tissue slides were dehydrated through a graded ethanol series, and antigen retrieval was performed using citrate buffer for 3 minutes. Citrate buffer was used to enhance antigen activity. Then, endogenous peroxidases in the tissue were inactivated with hydrogen peroxide in PBS for 5 minutes. In the next step, the slides were incubated with primary antibodies, including anti-MMP1, anti-elastin, anti-collagen type 1, anti-collagen type 2, anti-collagen type 3, and anti-TGF-β1 (1:100, Santa Cruz, USA), in a wet box at room temperature for 60 minutes. Then, the slides were incubated with biotinylated secondary antibodies and followed by Horseradish Peroxidase (HRP) for 10 minutes each at room temperature. Subsequently, the sections were dehydrated, mounted, and examined at 400× magnification under an optical microscope (Optilab Iris-4 Microscope Biology Trinocular, Miconos, Yogyakarta, Indonesia) with Optilab Viewer software. The expression of proteins was quantified using ImageJ 1.53e software (National Institutes of Health, Maryland, USA).

Statistical analysis

Data are presented as mean ± standard deviation (SD). Statistical analysis was performed using one-way analysis of variance (ANOVA), followed by Tukey's HSD test for post hoc multiple mean comparisons. A p-value of less than 0.05 or 0.01 was considered statistically significant. Analyses were performed using SPSS software (version 25.0, SPSS Inc., Chicago, IL, USA).

Results

HPLC method validation

Selectivity testing is conducted to ensure that the instrument used is capable of separating the target compound from impurities or other interfering substances while also ensuring that the target compound can be accurately analyzed and measured. The results of the curcumin and glycyrrhizin selectivity test are presented in Table 4. The chromatogram does not show any interference from other compound peaks on the curcumin peak (Fig. 1A, B) and exhibits the same spectral shape between the turmeric sample solution and the curcumin standard solution (Fig. 1C). The chromatograms of the glycyrrhizin standard and licorice extract show that the method used is selective (Fig. 2A, B) and exhibit the same spectral shape between the turmeric sample solution and the curcumin standard solution (Fig. 2C).

Table 4. Curcumin and glycyrrhizin selectivity test results.

Vial	λ (nm)	Rt	Rs	Tf
Standard curcumin 30 ppm	426	12.218	19.597	1.068
Turmeric extract		12.205	1.902	1.070
Standard glycyrrhizin 50 ppm	254	7.720	2.956	1.319
Licorice extract		7.742	2.099	1.341

Rt: retention time; Rs: resolution; Tf: Tailing factor.

A linearity test is conducted to ensure that the analytical method yields test results that are directly proportional to the sample concentration within a specified range. The calibration curves of curcumin and glycyrrhizin are shown in Fig. 3. The requirement for the correlation coefficient (r) in AOAC is 0.99 (AOAC 2023). Thus, it can be concluded that the linearity test on curcumin and glycyrrhizin meets this requirement. The results showed a satisfactory correlation between peak area response and concentration.

LOD is carried out to determine the lowest detectable limit of the analyte in the sample, but it cannot be measured as a definite, quantifiable value. LOQ is carried out to determine the detection limit of the amount of analyte from a sample whose value can be determined quantitatively based on a validated method (Indian Pharmacopoeia Commission 2021). LOD and LOQ data are obtained by

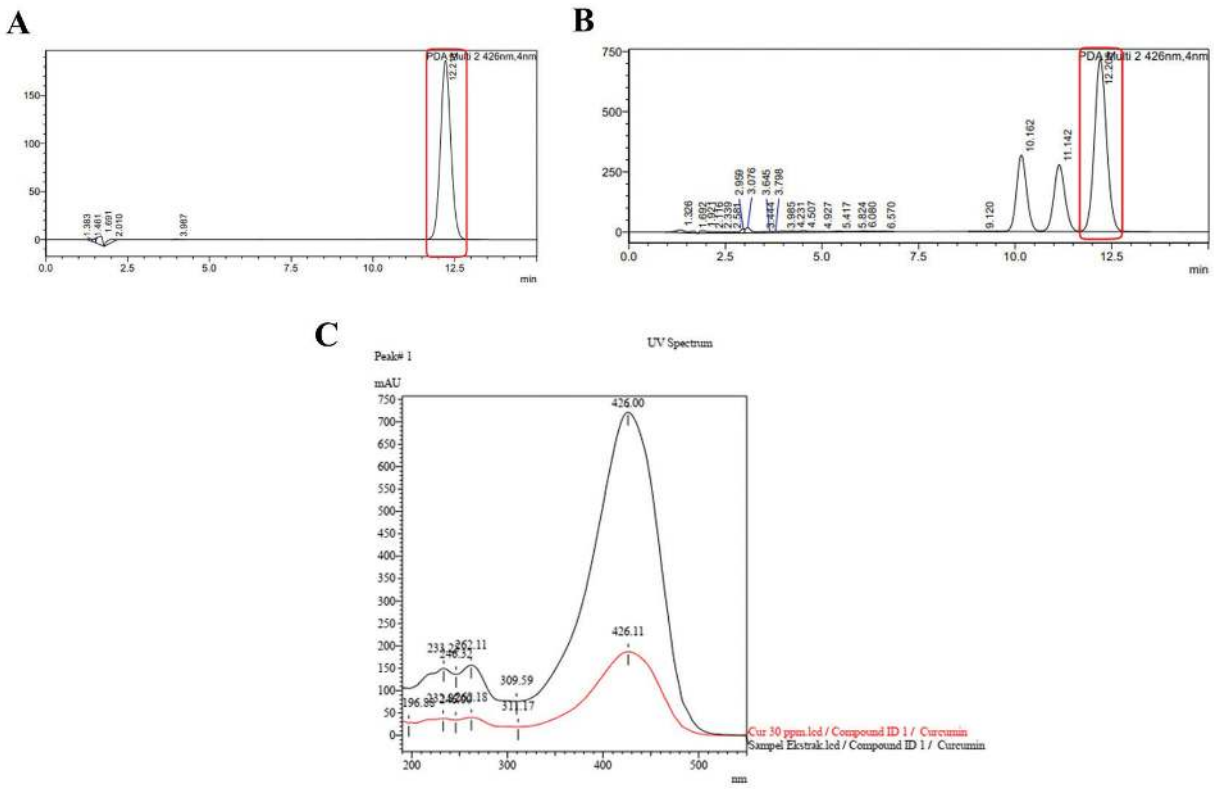


Figure 1. Chromatogram and UV spectrum comparison of curcumin in standard and turmeric extract. **A.** Chromatogram of the curcumin standard; **B.** Chromatogram of curcumin in the turmeric extract sample; **C.** Overlay of UV spectra comparing the curcumin standard and curcumin in the turmeric extract.

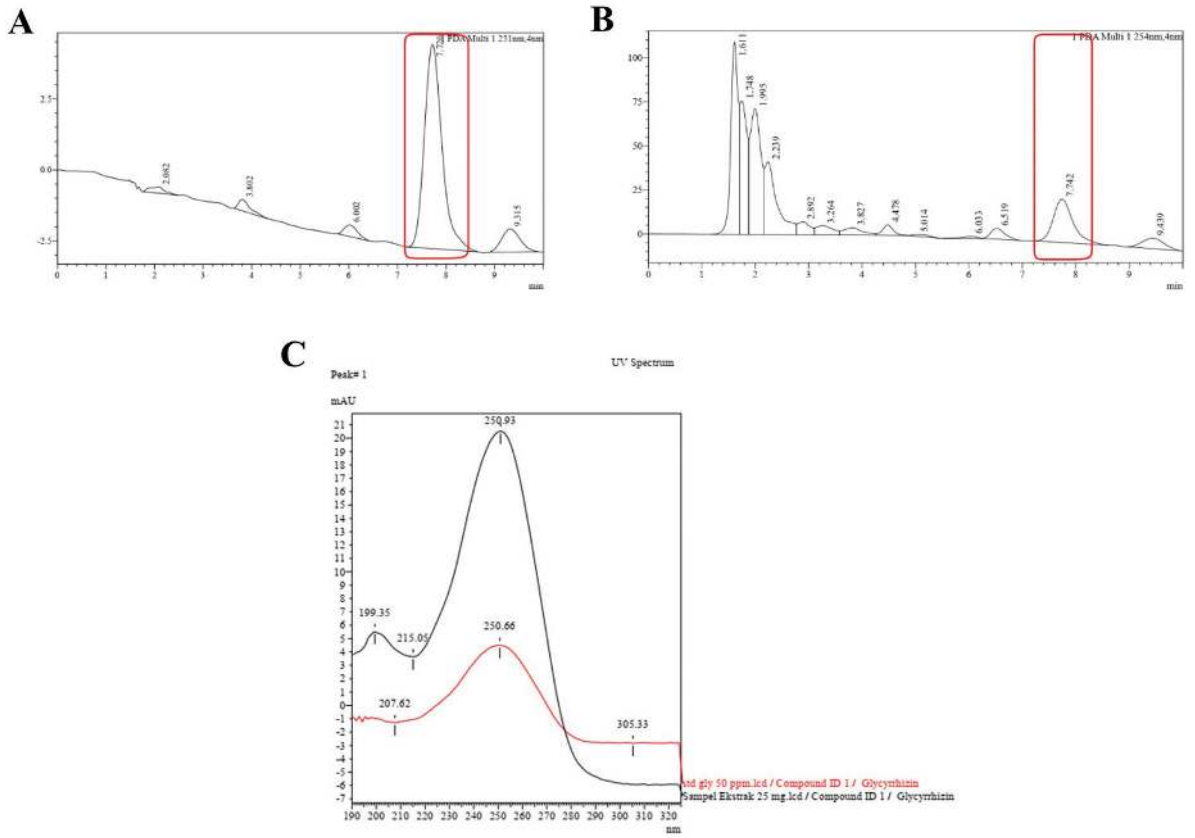


Figure 2. Chromatogram and UV spectrum comparison of glycyrrhizin in standard and licorice extract. **A.** Chromatogram of the glycyrrhizin standard; **B.** Chromatogram of glycyrrhizin in the licorice extract sample; **C.** Overlay of UV spectra comparing the glycyrrhizin standard and glycyrrhizin in the licorice extract.

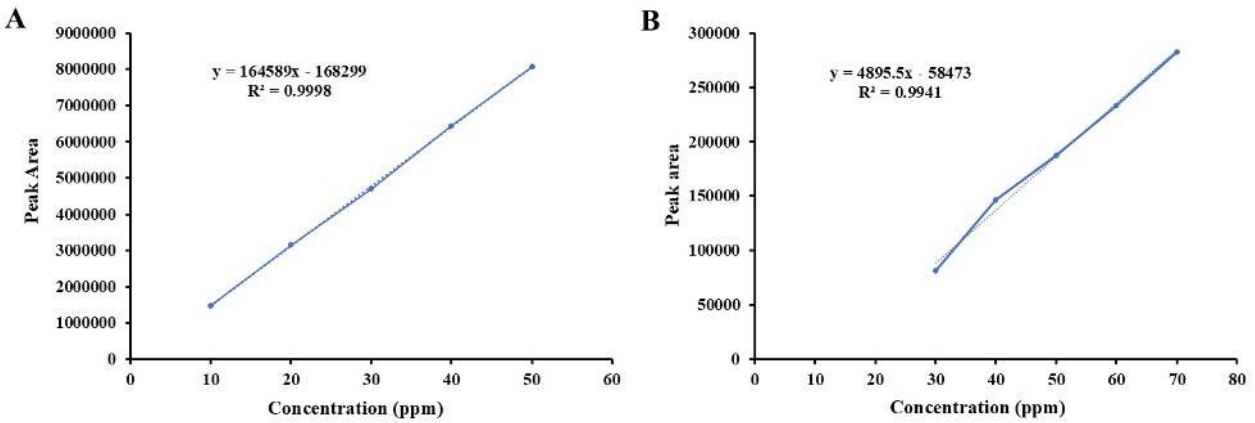


Figure 3. Calibration curve. **A.** Curcumin; **B.** Glycyrrhizin.

Table 5. Accuracy and precision test results of curcumin and glycyrrhizin.

Concentration in Sample (mg)	Standard addition (mg)	Theoretical concentration (ppm)	Measurable concentration (ppm)	% Recovery total	% RSD
Curcumin					
0.1	0.08	18	17.66	98.09	1.43
0.1	0.08	18	17.93	99.64	
0.1	0.08	18	18.17	100.96	
0.1	0.1	20	20.71	103.57	2.11
0.1	0.1	20	20.26	101.29	
0.1	0.1	20	19.86	99.29	
0.1	0.12	22	21.69	98.60	1.78
0.1	0.12	22	22.40	101.81	
0.1	0.12	22	21.75	98.87	
Glycyrrhizin					
0.3	0.24	54	52.96	98.07	1.48
0.3	0.24	54	52.58	97.37	
0.3	0.24	54	51.47	95.31	
0.3	0.3	60	58.26	97.11	1.88
0.3	0.3	60	59.38	98.96	
0.3	0.3	60	57.18	95.30	
0.3	0.36	66	63.88	96.78	0.56
0.3	0.36	66	63.25	95.83	
0.3	0.36	66	63.85	96.75	

calculating the regression equation using the standard deviation results from the regression formula that has been carried out. The LOD and LOQ values for curcumin are 0.862 ppm and 2.874 ppm, respectively. Meanwhile, the LOD and LOQ values for glycyrrhizin are 0.125 ppm and 0.418 ppm. Low LOD and LOQ values indicate adequate method sensitivity (Reddy et al. 2016). An accuracy precision test is conducted to determine the closeness between the values obtained from the test results and the reference values when the reference to determine the accuracy of the results is carried out repeatedly with the selected method from homogeneous samples. Accuracy is expressed as percent recovery, and precision is expressed in %RSD. The results of the accuracy and precision tests for curcumin and glycyrrhizin met the AOAC requirements. The AOAC requirements for 1% analyte are a %recovery in the range of 92–105% and a % RSD <2% (AOAC 2023). The results of the accuracy and precision of curcumin and glycyrrhizin using the addition method are shown in Table 5, confirming the previous results.

Determination of curcumin and glycyrrhizin contents was carried out on turmeric and licorice extracts used as the main components in the NLC and transfersome formulation. The results of the determination of curcumin and glycyrrhizin content in turmeric extract are shown in Table 6. The extraction yield of curcumin was 4.724%. These results indicate that the percentage of yield meets the requirements for the extraction yield of *Curcuma longa* rhizome simplicia listed in the Indonesian Herbal Pharmacopoeia (IHP) II, with a yield value of not less than 3.82%. Meanwhile, the extraction yield of glycyrrhizin was 7.096% (Minister of Health of the Republic of Indonesia 2017). These results indicate that the percentage of yield meets the requirements for the extraction yield of *Glycyrrhiza glabra* listed in WHO monographs, with a yield value of not less than 4% (World Health Organization 2002). Thus, this study fulfills this requirement.

Characterization of the Transfersome and NLC

The characterization of transfersome (TFS) and nanostructured lipid carrier (NLC) formulations revealed key parameters influencing their potential as effective transdermal delivery systems. As shown in Table 7, FT2 exhibited optimal particle size, PDI, and zeta potential among the TFS formulations. Smaller and more uniform particles are essential for enhanced skin penetration and reduced aggregation during storage. The negative zeta potential in FT2 also suggests improved colloidal stability, likely due to the presence of non-ionic surfactants such as Tween 80, which confer steric and electrostatic stabilization. Among NLC formulations, FN3 showed the most favorable physicochemical profile, with reduced particle size and acceptable PDI compared with FN1 and FN2. The improved performance of FN3 may be attributed to its higher proportion of liquid lipid, which enhances matrix imperfections and promotes better incorporation and dispersion of active compounds.

Deformability is a critical parameter for vesicular carriers intended for dermal application, as it facilitates passage through the stratum corneum and ensures deeper skin penetration without compromising vesicle integrity. The deformability test (Table 8) confirmed the high flexibility of FT2 vesicles, as reflected in their deformability percent and index.

Encapsulation data in Table 9 showed that both TFS and NLC systems achieved substantial entrapment of curcumin and glycyrrhizin, with FT2 and FN3 consistently demonstrating the highest entrapment efficiency and

Table 6. Results of determination of curcumin and glycyrrhizin contents.

Replication	Amount of sample taken (mg)	Concentrations in 25 mL (ppm)	Content in 25 mL (mg)	% w/w	% RSD
Curcumin					
1	25	116.794	1.168	4.672	1.04
2	25	119.745	1.197	4.790	
3	25	117.739	1.177	4.710	
	Average	118.093	1.181	4.724	
Glycyrrhizin					
1	62.5	440.376	4.404	7.046	1.42
2	62.5	452.276	4.523	7.236	
3	62.5	427.831	4.378	7.005	
	Average	443.494	4.435	7.096	

Table 7. Physical characterization of TFS and NLC.

Formula		Particle size (nm)	Polydispersity index	Zeta potential (mV)
TFS	FT1	197.48 ± 11.41	0.45 ± 0.08	2.22 ± 4.93
	FT2	172.61 ± 37.71	0.45 ± 0.01	-1.09 ± 6.90
	FT3	194.71 ± 18.58	0.47 ± 0.10	-1.73 ± 3.35
NLC	FN1	737.22 ± 147.18	0.45 ± 0.27	-2.35 ± 0.57
	FN2	312.22 ± 77.31	0.57 ± 0.24	-2.02 ± 1.9
	FN3	196.22 ± 130.47	0.44 ± 0.27	-3.75 ± 1.95

Table 8. Deformability test results of TFS.

Formula		Particle size before extrusion (nm)	Particle size after extrusion (nm)	Deformability percent (%)	Deformability index
TFS	FT1	197.48 ± 11.41	147.75 ± 11.21	74,75 ± 1.95	10.70 ± 1.67
	FT2	172.61 ± 37.71	128.83 ± 36.67	73.69 ± 5.20	8.71 ± 4.78
	FT3	194.71 ± 18.58	152.02 ± 14.94	78.05 ± 0.24	11.48 ± 2.03

Table 9. Entrapment efficiency and drug loading for TFS and NLC.

Formula		Entrapment efficiency		Drug loading	
		Curcumin (%)	Glycyrrhizin (%)	Curcumin (%)	Glycyrrhizin (%)
TFS	FT1	75.82 ± 7.42	24.56 ± 1.37	0.72 ± 0.07	0.35± 0.02
	FT2	57.83 ± 2.98	26.32 ± 1.32	0.55 ± 0.03	0.37 ± 0.02
	FT3	56.77 ± 2.20	27.32 ± 1.29	0.54 ± 0.02	0.39 ± 0.02
NLC	FN1	71.27 ± 7.46	71.32 ± 2.58	0.32 ± 0.03	0.49 ± 0.02
	FN2	75.43 ± 3.97	67.41 ± 3.49	0.34 ± 0.02	0.46 ± 0.02
	FN3	80.53 ± 4.93	66.19 ± 2.59	0.36 ± 0.02	0.45 ± 0.02

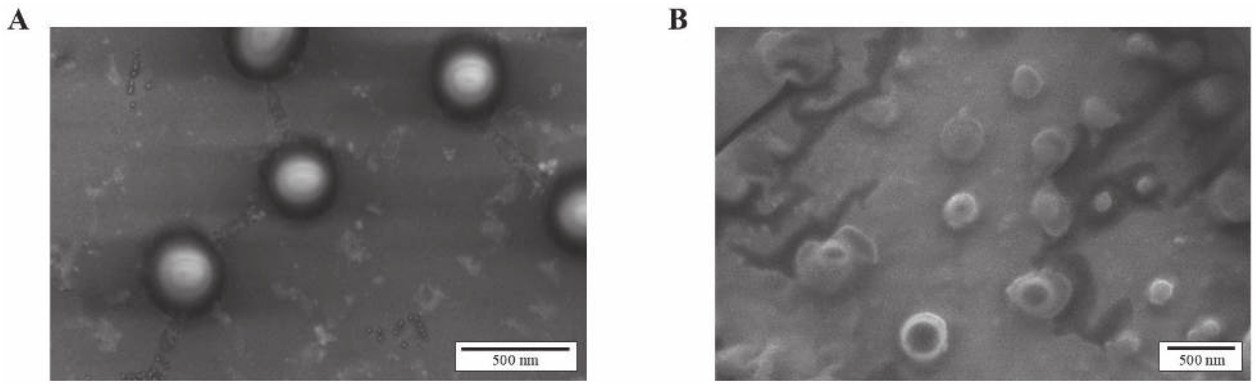


Figure 4. Surface morphology using an SEM. **A.** TFS-CGE, magnification: 5000×; **B.** NLC-CGE, magnification: 3000×.

drug loading. These findings reinforce their suitability for delivering hydrophobic and amphiphilic bioactives in anti-aging formulations.

Based on the overall results, FT2 and FN3 were selected as the optimal formulations for further investigation. As shown in Fig. 4, both FT2 and FN3 exhibited spherical morphology, which further supports their suitability as nanocarrier systems for topical application.

in vitro anti-aging activity

The *in vitro* anti-aging activity was evaluated using antioxidant and collagenase inhibition assays. The antioxidant activity was determined using the DPPH radical scavenging assay, with each test conducted in triplicate. The results in Table 10 are presented as half-maximal inhibitory concentration (IC_{50}) values, where a lower IC_{50} value indicates stronger antioxidant activity. The antioxidant activity is also expressed as an inhibition percentage at an 80 ppm concentration (Fig. 5A), where a higher inhibition percentage indicates a greater antioxidant capacity. Based on the results, the antioxidant activity ranking from highest to lowest is as follows: turmeric extract, NLC, a combination of turmeric and licorice extracts, licorice extract, and transfersome. Collagenase inhibition activity was measured based on the percentage of inhibition at 80 ppm. As shown in Fig. 5B, the highest collagenase inhibition activity was observed in the following order: NLC > licorice extract > turmeric and licorice extracts combination > transfersome > turmeric extract.

Table 10. Antioxidant activity of extracts, transfersomes, and NLC.

Sample	IC_{50} for DPPH (ppm)
Transfersome (TFS-CGE)	128.242
NLC (NLC-CGE)	51.519
Turmeric extract (C extract)	44.370
Licorice extract (G extract)	100.179
Turmeric and licorice extract (CGE)	52.444

Gel physical stability study

The transfersome and NLC gel preparations were also evaluated for physical stability over 30 days of storage. The pH, viscosity, and appearance of the TFS and NLC gels were evaluated, and the data are presented in Table 11. During storage of the TFS and NLC gels, all evaluations revealed no significant changes after 30 days of storage.

MED determination

The minimal erythema dose (MED) was determined by exposing rat dorsal skin to UV-B radiation at varying durations (5, 10, 15, 20, 30, and 60 minutes), as shown in Fig. 6. Erythema was observed 48 hours post-irradiation, and the area exposed for 10 minutes demonstrated the first visible signs of minimal redness, which was designated as 1 MED (135 mJ/cm^2) for subsequent UV-B exposure protocols.

Effect of TFS and NLC gels on rat skin appearance

Fig. 7 presents the macroscopic appearance of rat dorsal skin following UV-B exposure and treatment. The control group exhibited smooth, healthy skin, while the UV-B group showed visible erythema, indicating the signs of photoaging. Treatment with TFS-CGE and NLC-CGE gels improved skin appearance, resulting in reduced redness and a smoother texture compared with the UV-B group. In contrast, the TFS base and NLC base gel groups showed no visible improvement, with persistent erythema and roughness similar to the UV-B group. The CGE gel also failed to restore skin appearance, with visible wrinkling and uneven texture observed.

Effect of TFS and NLC on skin elasticity

Skin elasticity was evaluated weekly using the pinch test, which measured the time required for the stretched skin to return to its original position. As shown in Fig. 8, UV-B irradiation progressively impaired skin elasticity, with significantly longer recovery times observed in the UV-B group compared with the control group across all weeks. In contrast, the TFS-CGE gel, NLC-CGE gel, and base gel groups had significant differences compared with the UV-B group at weeks one and three, whereas the second week showed no significant difference. In addition, the TFS-CGE gel group showed significant differences

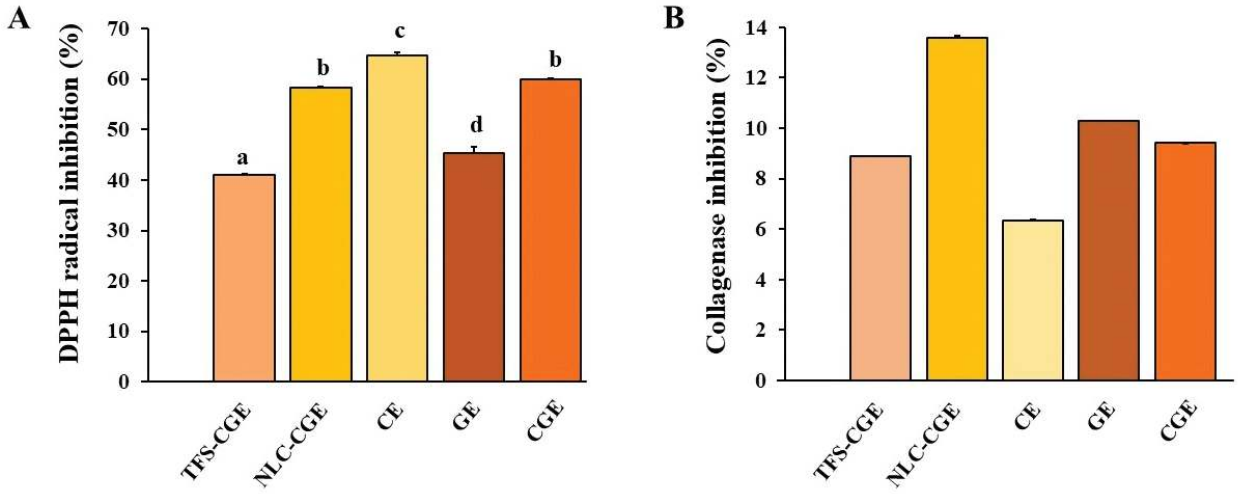


Figure 5. *In vitro* antioxidant and anticollagenase activity. **A.** Antioxidant; **B.** Collagenase. The concentration of the sample used was 80 ppm. The difference in letters shows that the result was significantly different with $p < 0.05$.

Table 11. Assessment of the physical stability of gels in 30 days.

Sample	pH		Viscosity (cP)		Appearance	
	Day 0	Day 30	Day 0	Day 30	Day 0	Day 30
TFS-CGE gel	5.256 ± 0.03	5.260 ± 0.04	31666 ± 3214	30666 ± 2516	+++	+++
NLC-CGE gel	5.500 ± 0.07	5.476 ± 0.09	34333 ± 1527	29666 ± 3055	+++	+++
TFS base gel	5.570 ± 0.03	5.640 ± 0.08	30333 ± 2516	32000 ± 1000	+++	+++
NLC base gel	6.383 ± 0.04	6.263 ± 0.20	31666 ± 3214	31000 ± 2645	+++	+++
CGE gel	5.963 ± 0.08	5.950 ± 0.10	38333 ± 1527	39000 ± 3000	+++	+++

+++ good, ++ average, + poor; data are represented as mean ± SD (n = 3).

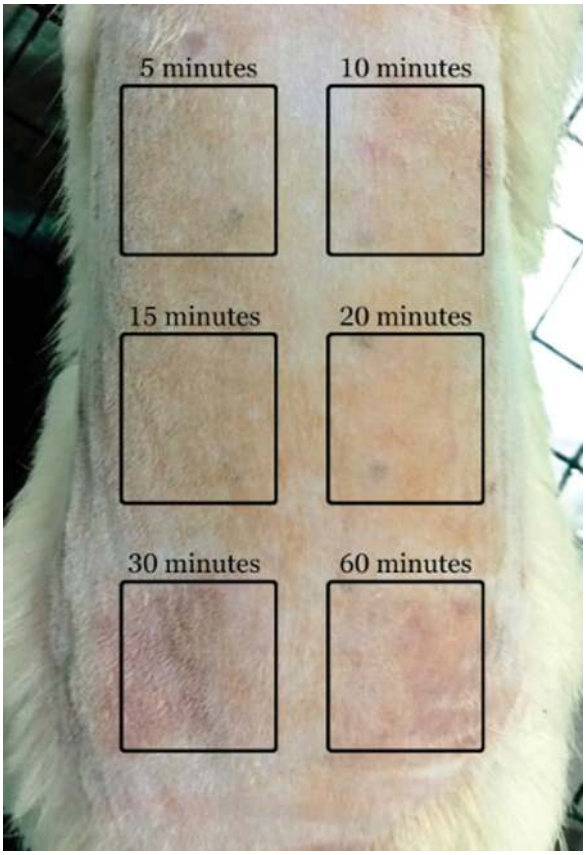


Figure 6. MED determination.

compared with the base gel group in the second and third weeks. The NLC-CGE gel group showed no significant difference compared with the NLC base gel group at week two but exhibited a difference at week three. Starting from the second week, the GCE gel group showed a significant difference compared with the TFS-CGE gel and NLC-CGE gel groups. However, the NLC-CGE gel group had a lower recovery time in the third week.

Effect of TFS and NLC gels on epidermal thickness and collagen density

Histological analysis with H&E staining (Fig. 9A) revealed that UV-B exposure resulted in a significant increase in epidermal thickness compared with the control group (Fig. 9B). The use of TFS-CGE and NLC-CGE gels significantly decreased epidermal thickening, with both formulations showing prominent results. In contrast, the TFS and NLC base gels, as well as the CGE gel, resulted in only slight improvements. Masson's trichrome staining (Fig. 9C) demonstrated a reduction in collagen density within the UV-B exposure group. However, treatment with TFS-CGE and NLC-CGE gels resulted in a significant enhancement of collagen levels in the dermis (Fig. 9D), with NLC-CGE exhibiting the most significant increase. In contrast, the collagen restoration observed in the CGE and base gel groups was inferior compared with that of the nanocarrier-based formulations.

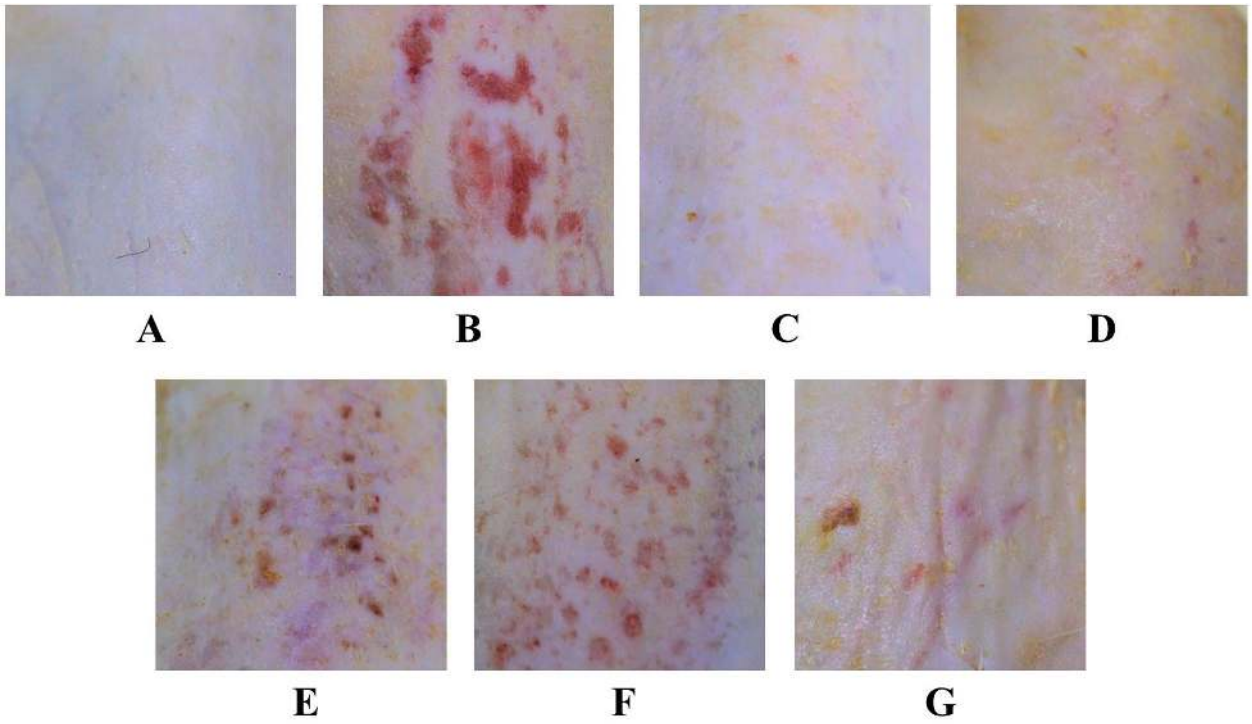


Figure 7. Photographs of the dorsal skin of rats. **A.** Normal skin; **B.** Skin after induction of UV-B; **C.** Skin after induction of UV-B and treatment with TFS-CGE gel; **D.** Skin after induction of UV-B and treatment with NLC-CGE gel; **E.** Skin after induction of UV-B and treatment with TFS gel base (without extracts); **F.** Skin after induction of UV-B and treatment with NLC gel base (without extracts); **G.** Skin after induction of UV-B and treatment with gel extract.

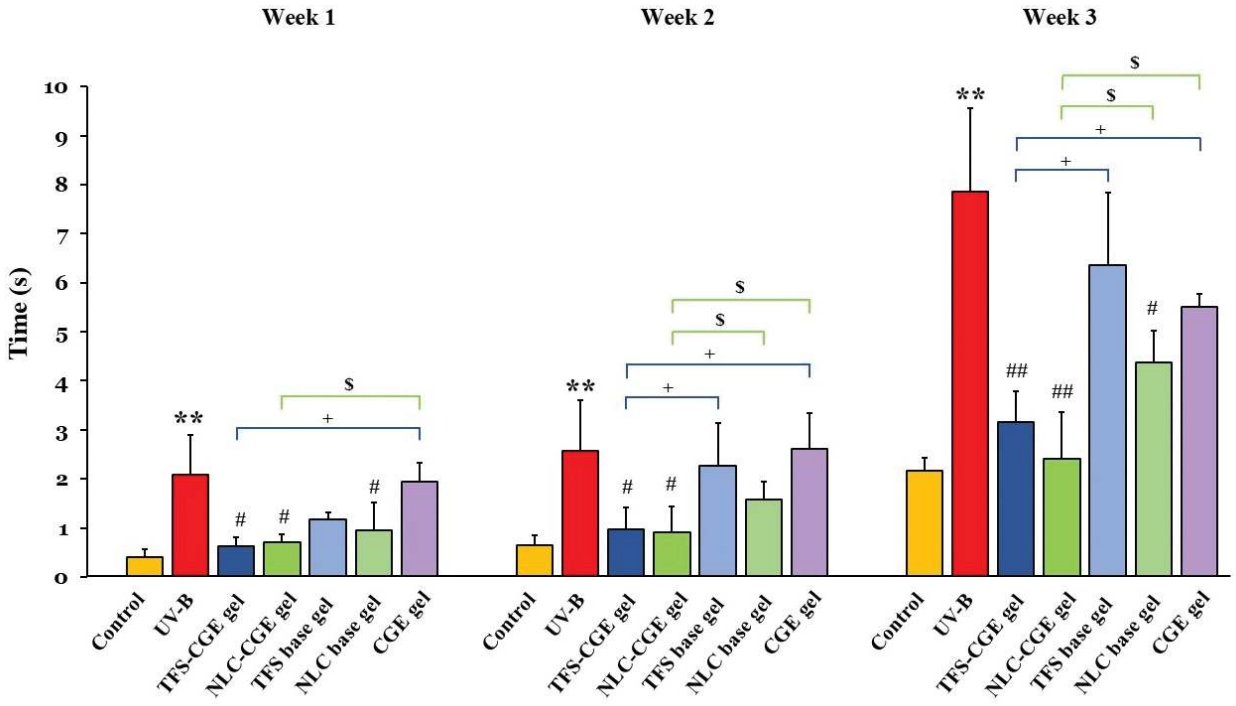


Figure 8. Effect of transfersome and NLC gels on skin elasticity. Data represented as mean ± SD. Statistical analysis was performed using one-way ANOVA and the post-hoc Tukey-HSD test. * statistically significant from the control group $p < 0.05$; ** statistically significant from the control group $p < 0.001$; # statistically significant from the UV-B group $p < 0.05$; ## statistically significant from the UV-B group $p < 0.05$; + statistically significant from the TFS-CGE gel group $p < 0.05$; ++ statistically significant from the TFS-CGE gel group $p < 0.001$; $ statistically significant from the NLC-CGE gel group $p < 0.05$; $$ statistically significant from the NLC-CGE gel group $p < 0.001$.

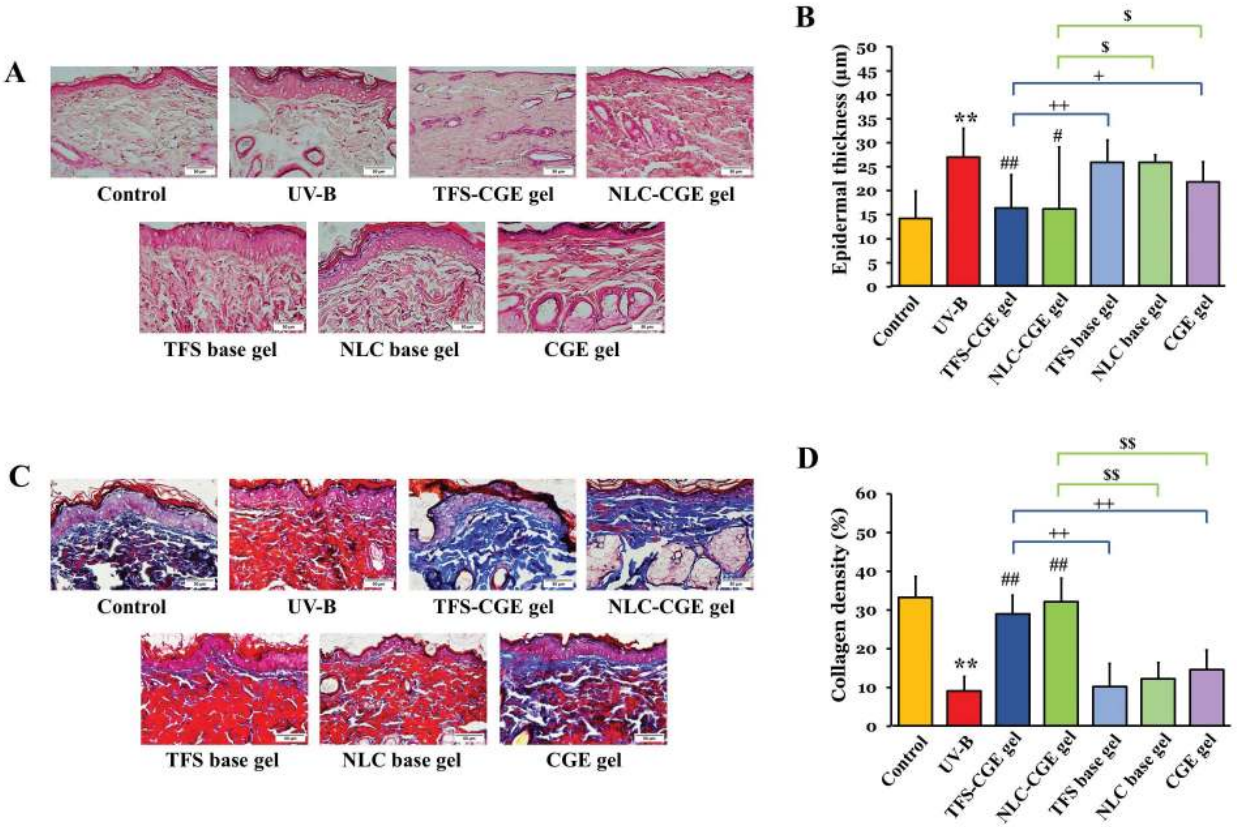


Figure 9. Effect of transfersome and NLC gels on the epidermal thickness and collagen density. **A.** Representative H&E staining of skin tissue; **B.** Quantitative analysis of epidermal thickness; **C.** Representative Masson's trichrome staining of skin tissue; **D.** Quantitative analysis of collagen density. Data represented as mean ± SD. Statistical analysis was carried out by one-way ANOVA and post-hoc Turkey-HSD. * statistically significant from the control group $p < 0.05$; ** statistically significant from the control group at $p < 0.001$; # statistically significant from the UV-B group $p < 0.05$; ## statistically significant from the UV-B group $p < 0.05$; + statistically significant from the TFS-CGE gel group $p < 0.05$; ++ statistically significant from the TFS-CGE gel group $p < 0.001$; $ statistically significant from the NLC-CGE gel group $p < 0.05$; $$ statistically significant from the NLC-CGE gel group $p < 0.001$.

Effect of TFS and NLC gels on expression of TGF-β1, MMP-1, and elastin

Exposure to UV-B resulted in a significant decrease in the expression of TGF-β1 and elastin, along with a marked increase in MMP-1 expression, indicating skin damage and matrix degradation. As shown in Fig. 10, treatment with TFS-CGE and NLC-CGE gels significantly reversed these effects, with higher expressions of TGF-β1 and elastin and lower expression of MMP-1 compared with the UV-B group. The CGE gel group showed a moderate improvement, whereas the base gel groups, which did not contain active extracts, exhibited minimal changes and showed expressions that were not significantly different from the UV-B group.

Effect of TFS and NLC gels on expression of collagen types I, II, and III

UV radiation caused a significant reduction in the expression of collagen types I, II, and III compared with the normal control group. The TFS-CGE and NLC-CGE gels significantly restored the expression of all three collagen types relative to the UV-B group. Furthermore, both nanocarrier-based formulations demonstrated superior efficacy in enhancing collagen I, II, and III expression compared with the CGE gel, as well as the TFS and NLC base gels, as shown in Fig. 11.

Discussion

Transfersome and NLC turmeric and licorice extracts were prepared using three formulas based on differences in critical parameters of each preparation. In this study, the TFS formula optimized the concentration of phospholipids and surfactant with ratios of 85:15, 80:20, and 75:25, while the NLC formula optimized the concentration of liquid lipids and solid lipids with ratios of 90:10, 80:20, and 70:30. TFS was prepared using the thin-layer hydration method with additional modifications to the sonication and extrusion steps. The thin-layer hydration method was chosen because it is easy to handle and provides a high level of active substance encapsulation. The

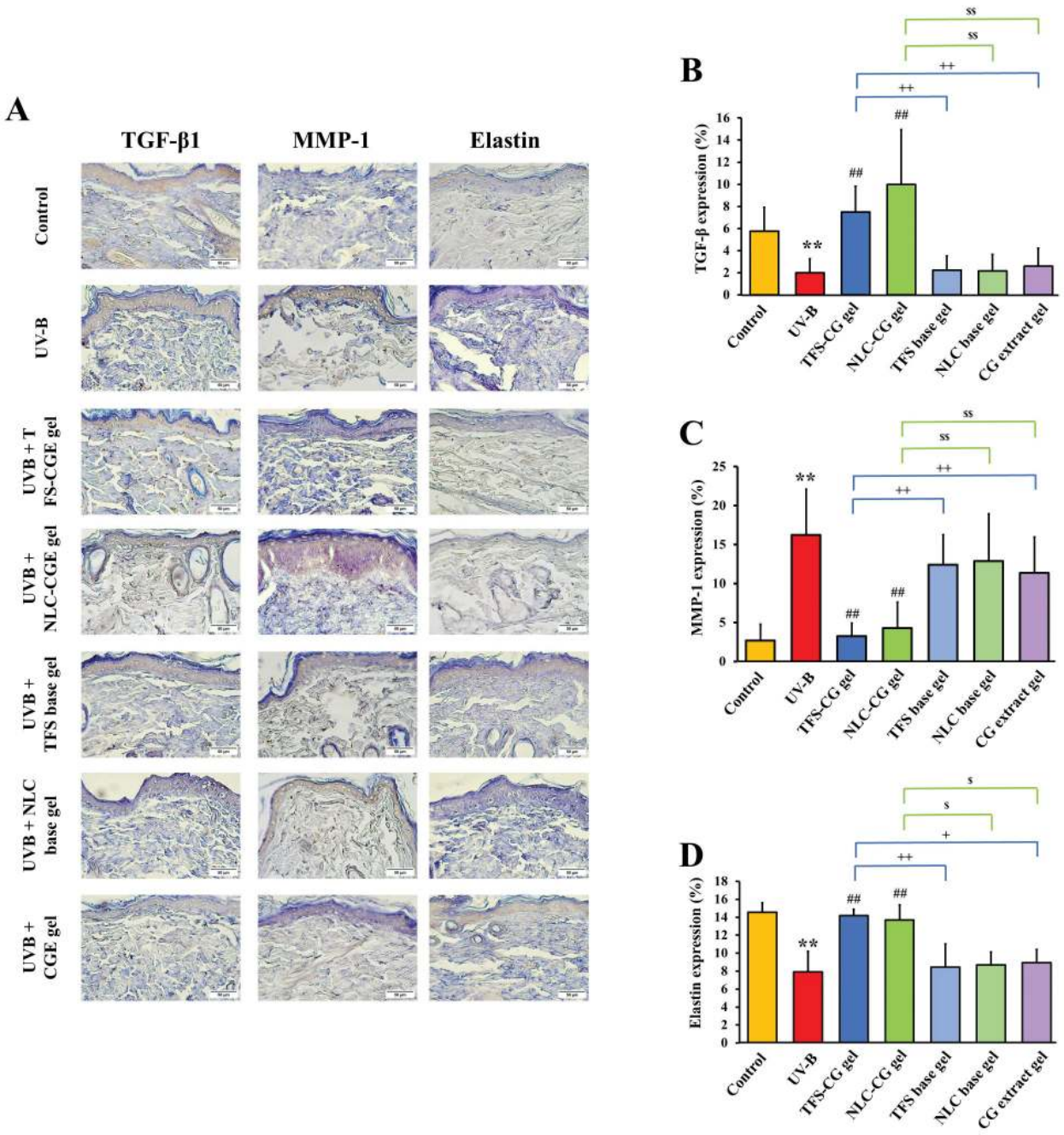


Figure 10. Effect of transfersome and NLC gels on the expression of TGF-β1, MMP-1, and elastin. **A.** Representative immunohistochemistry staining of TGF-β1, MMP-1, and elastin; **B.** Quantitative analysis of TGF-β1 expression; **C.** Quantitative analysis of MMP-1 expression; **D.** Quantitative analysis of elastin expression. Data represented as mean ± SD. Statistical analysis was carried out by one-way ANOVA and post-hoc Turkey-HSD. * statistically significant from the control group $p < 0.05$; ** statistically significant from the control group at $p < 0.001$; # statistically significant from the UV-B group $p < 0.05$; ## statistically significant from the UV-B group $p < 0.05$; + statistically significant from the TFS-CGE gel group $p < 0.05$; ++ statistically significant from the TFS-CGE gel group $p < 0.001$; $ statistically significant from the NLC-CGE gel group $p < 0.05$; $$ statistically significant from the NLC-CGE gel group $p < 0.001$.

sonication stage was selected because of its high efficiency in reducing particle size. In preparing TFS, sonication duration is one of the critical parameters (Fernández-García et al. 2020). The extrusion stage is carried out to reduce particle size and the TFS polydispersity index (Khan et al. 2021), thereby homogenizing the particle size. The advantage of the extrusion method is its ease of scale-up (applicable on an industrial scale) and its reproducible particle size reduction. In the extrusion stage, the hydration products are passed through pores under constant pressure to break multilamellar vesicles into unilamellar vesicles (Fernández-García et al. 2020). In the process of making TFS using the thin-layer hydration method, there are critical parameters at each stage. The critical parameters at

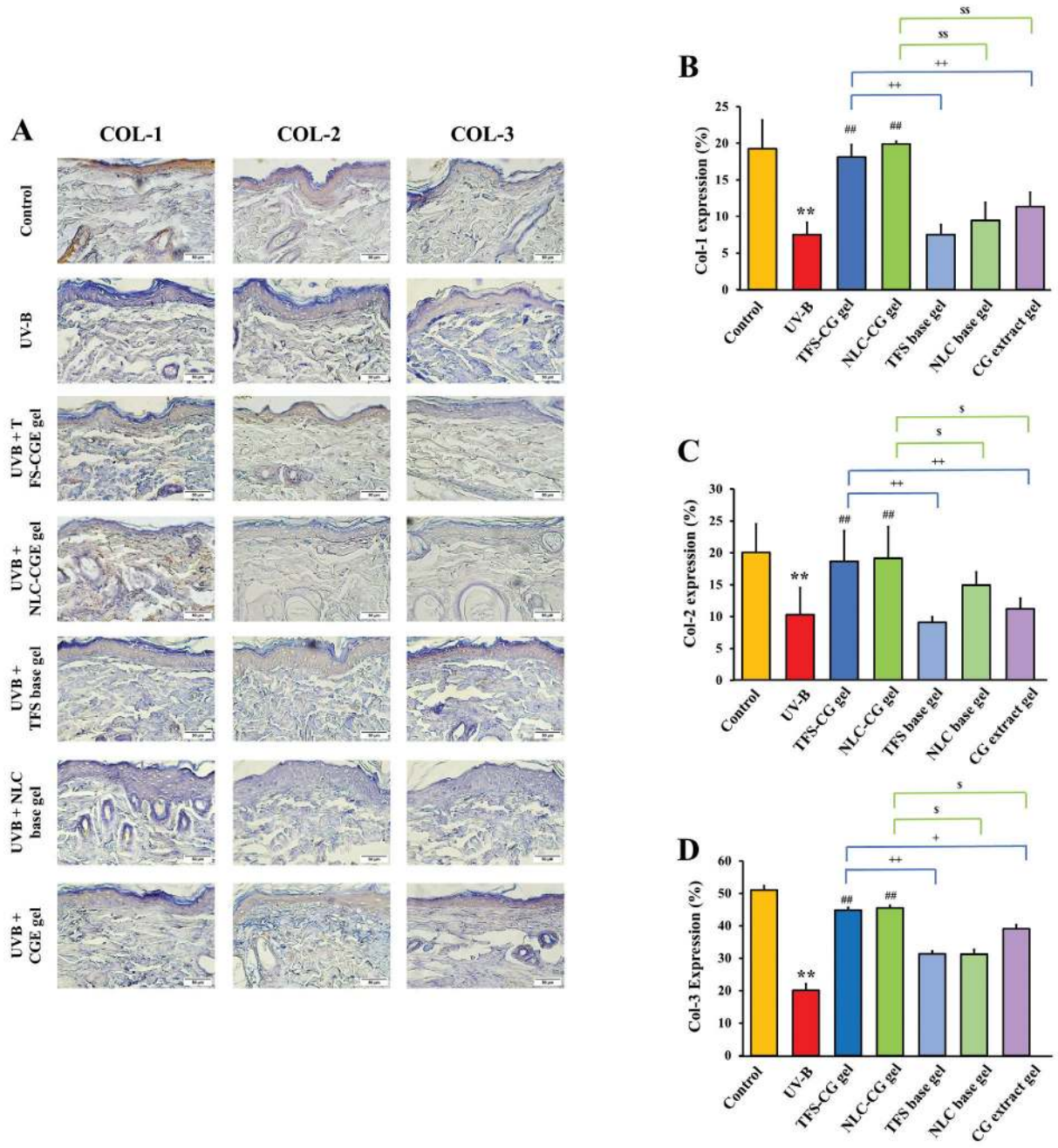


Figure 11. Effect of transfersome and NLC gels on the expression of collagen types I, II, and III. **A.** Representative immunohistochemistry staining of collagen types I, II, and III; **B.** Quantitative analysis of type I collagen expression; **C.** Quantitative analysis of type II collagen expression; **D.** Quantitative analysis of type III collagen expression. Data represented as mean ± SD. Statistical analysis was carried out by one-way ANOVA and post-hoc Turkey-HSD. * statistically significant from the control group $p < 0.05$; ** statistically significant from the control group at $p < 0.001$; # statistically significant from the UV-B group $p < 0.05$; ## statistically significant from the UV-B group $p < 0.05$; + statistically significant from the TFS-CGE gel group $p < 0.05$; ++ statistically significant from the TFS-CGE gel group $p < 0.001$; $ statistically significant from the NLC-CGE gel group $p < 0.05$; $$ statistically significant from the NLC-CGE gel group $p < 0.001$.

the lipid phase dissolution stage include lipid solubility, solvent amount, dissolution temperature, and the addition of lipophilic active substances (such as turmeric extract). Critical parameters in the evaporation stage include temperature, pressure, rotation speed, and duration. The critical parameters at the hydration stage are the amount of hydration medium and the addition of hydrophilic active substances (licorice extract). The critical parameters at the sonication stage are frequency, temperature, and duration. The critical parameters at the extrusion stage are the number of filtration cycles and the pore size of the filter membrane. Among these parameters, temperature, sonication duration, and filtration amount have the greatest influence on the final product (Németh et al. 2021).

NLC was produced using hot emulsification and ultrasonication. This procedure has the advantage of being relatively simple and does not require organic solvents (Subramaniam et al. 2020). The critical parameters in making NLC are heating, stirring, and crystallization. Heating must be controlled to maintain drug stability against oxidation (Weiss et al. 2008). Stirring plays a crucial role in achieving homogeneous dispersion and uniform particle distribution, significantly affecting NLC quality (Shimojo et al. 2019). The degree of crystallization during NLC formation also influences encapsulation efficiency (Chauhan et al. 2020). Based on the evaluation results, FT2 was the optimal TFS formula. This is because the phospholipid-to-surfactant ratio produced vesicles capable of effectively absorbing active substances. FN3 was the optimal NLC preparation in this study because the higher proportion of liquid lipids facilitated better absorption of the active substances. Based on the TFS particle measurement results, the three formulas did not differ significantly. All had particle sizes below 200 nm. A previous study on turmeric extract TFS cream reported that TFS with particle sizes ranging from 100 to 400 nm could penetrate the skin and accumulate in the dermis layer (Saraf et al. 2011). The three TFS formulas in this study fell within this particle size range, meeting the requirements for dermal delivery of active substances. Among them, TFS with an 80:20 ratio had the smallest particle size. In TFS with ratios of 85:15 and 80:20, higher surfactant levels led to smaller particle sizes. However, exceeding the surfactant limit, as in the 75:25 ratio, caused an increase in particle size. When compared with the 85:15 ratio, the 80:20 ratio had less phospholipid and more Tween 80 surfactant.

The amount of surfactant can affect TFS particle size. Tween 80 contains an ethylene oxide side chain, which inhibits vesicle aggregation by providing steric repulsion in the aqueous phase. The shorter lipophilic segment of Tween 80 causes shallow insertion into the bilayer, increasing vesicle curvature as the hydrophilic head expands outward. This reduces the hydrophobic portion of the TFS bilayer and results in smaller particle sizes (Taymouri et al. 2021). Reducing phospholipid content decreases vesicle constituents, and high surfactant concentrations further reduce particle size (Khan et al. 2015).

In this study, TFS with a ratio of 75:25 had a larger particle size than TFS with a ratio of 80:20. The increase in vesicle size occurs because the use of surfactant exceeds the optimum limit of surfactant concentration in TFS, namely 20%. The use of surfactant at concentrations above 20% results in the formation of micelles in the double layer, which leads to the formation of pores in the vesicle membrane (Gupta et al. 2012). Other research also shows a similar trend. There was an increase in particle size in the TFS formulation with phospholipid-to-surfactant ratios of 75:25 and 55:45 compared with 95:5. This increase in size occurs due to the large amount of surfactant used, which may cause molecular repulsion between the surfactant and phospholipid molecules in the TFS bilayer (Bnyan et al. 2019). Particle size and polydispersity index can affect the stability of TFS and NLC. A smaller particle size exhibits less aggregation over time. Particle size also influences solubility, biocompatibility, and drug release rate (Haider et al. 2020). The polydispersity index is a parameter used to measure the uniformity of particle size distribution. PDI values range from 0.0 to 1.0. A value of 0.0 indicates that the sample has perfectly homogeneous particle sizes, whereas a value of 1.0 indicates that the sample has very heterogeneous particle sizes with several particle size populations (Khan et al. 2022). In this study, the TFS PDI value increased with the increasing amount of surfactant, from ratios of 85:15, 80:20, and 75:25, respectively. There were no significant differences ($p > 0.05$) between the three TFS formulations. The polydispersity index of the three formulas meets the specification, namely less than 0.5, which represents a relatively uniform particle size distribution (El-Gizawy et al. 2020; Chabru et al. 2024).

Zeta potential measurements were performed to determine the potential difference in a particle, which affects the aggregation process and physical stability. Preparations that have a positive or negative charge will exhibit electrostatic repulsion between particles in close proximity. A good zeta potential is higher than +30 mV or lower than −30 mV (Gomaa et al. 2022). In this study, the three TFS formulations exhibited a zeta potential close to 0, and the zeta potential value of TFS decreased to become more negative as the surfactant was added. However, there was no significant difference ($p > 0.05$) between the three formulas. The zeta potentials of the three formulas fall within the range of +10 mV to −10 mV, so they can be considered neutrally charged (Khan et al. 2021). The zeta potential value mainly depends on the charge of the lipids and surfactants that make up the TFS (Al Shuwaili et al. 2016). This research uses the nonionic surfactant Tween 80. Tween 80 can give a negative charge on the surface due to partial hydrolysis of the polyethylene oxide head group ((CH2-CH2-O)n) (Ahad et al. 2018). Therefore, the zeta potential charge decreases as the amount of Tween 80 increases. The use of soy lecithin, which contains phosphatidylcholine, can also affect the zeta potential value. Phosphatidylcholine has an isoelectric point between 6 and 7, resulting in a slightly negative charge in PBS medium at pH 7.4, which is above its isoelectric point (Dhavale et al. 2021). The fact that none of the three formulas has a completely neutral zeta potential charge may be caused by small amounts of impurities, such as phospholipid impurities from impure soy lecithin or active ingredients from the extract. Morphological analysis of TFS and NLC was carried out using FESEM with samples in the form of liquid dried at room temperature. Morphological analysis was performed on the optimal formulation for each preparation. The results of the SEM analysis indicate that the TFS vesicles and NLC nanoparticles are spherical in shape, which can enhance the penetration of active substances through the stratum corneum (Ghasemiyeh and Mohammadi-Samani 2018).

The deformability characteristics of TFS were presented by the deformability index and percent deformability. The deformability index shows the TFS ability to pass through

a pore of smaller size (Garg et al. 2017). This shows that TFS with a ratio of 85:15 can pass through pores 10.70 times smaller than its size. TFS with a ratio of 80:20 can pass through pores 8.71 times smaller than its size. TFS with a ratio of 75:25 can pass through pores 11.48 times smaller than its size. When compared with the size of the vesicle after extrusion, the smaller the vesicle size, the smaller the vesicle deformability index value. The percent deformability value shows the flexibility of the TFS to return to its original size (Goindi et al. 2013). The closer it is to 100%, the better the TFS ability to return to its original size before extrusion (Garg et al. 2017; Das et al. 2023). TFS with a ratio of 85:15 can return to the original TFS size of 74.75 ± 1.95%. In other words, the TFS decreased in size by 25.25 ± 1.95% after the extrusion process. Meanwhile, TFS with ratios of 80:20 and 75:25 experienced decreases in size of 26.31 ± 5.20% and 21.95 ± 0.24%, respectively. Based on this value, TFS with a ratio of 75:25 is the most flexible formula because it has the least reduction in particle size compared with the other formulas.

Two active compounds are used in this research, licorice extract and turmeric extract. Curcumin entrapment efficiency and drug loading were determined using an indirect method. From the results obtained, the entrapment efficiency and drug loading values decreased as the TFS phospholipid-to-surfactant ratio decreased (85:15, 80:20, and 75:25). TFS with a ratio of 85:15 had significant differences in EE and DL values ($p < 0.05$) compared with TFS with ratios of 80:20 and 75:25. The greater the amount of phospholipids and the smaller the amount of surfactant, the higher the EE and DL values. The greater the amount of phospholipids, the greater the active substance that can enter the vesicles. Phospholipids are an important component of vesicles. More phospholipids might facilitate the entry of active substances into the lipid bilayer (Khatoon et al. 2019). On the other hand, the addition of surfactant causes the formation of pores in the bilayer. The addition of surfactant at concentrations greater than 15% causes the formation of small and stiff micelles, thereby reducing the adsorption of active substances (El Zaafarany et al. 2010).

Fig. 12 illustrates the proposed molecular mechanism by which TFS-CGE and NLC-CGE gels exert protective effects against UV-B-induced photoaging. UV-B radiation absorbed by epidermal cells induces the formation of reactive oxygen species (ROS), which trigger oxidative stress and activate the MAPK signaling pathway. This activation subsequently induces AP-1, a transcription factor that increases the expression of MMP-1, MMP-3, and MMP-9, key enzymes responsible for the degradation of collagen types I, II, and III (Wei et al. 2024). Additionally, AP-1 activation enhances SMAD7 expression, which interferes with the TGF-β signaling pathway by binding to TβRI and preventing the formation of the TGF-β-TβRI-TβRII complex (Quan et al. 2005). Under normal physiological conditions, ROS can activate TGF-β, which binds to TβRII and activates TβRI through phosphorylation. This leads to the formation of the TGF-β-TβR1-TβRII complex, allowing SMAD2/3 to be recruited via the SMAD anchor for receptor activation (SARA). The R-SMADs then oligomerize with SMAD4 and translocate into the nucleus to promote the transcription of collagen types I, II, and III, as well as elastin and TGF-β (Deng et al. 2024). However, increased SMAD7 activity competitively inhibits SMAD2/3 from binding to SMAD4 and also directly interferes with TβRI binding. This disruption suppresses collagen gene transcription, leading to a reduction in extracellular matrix (ECM) production (Miyazawa and Miyazono 2017). Furthermore, UV-B exposure downregulates TBRII expression, further impairing the TGF-β signaling pathway (Quan et al. 2001).

Treatment with transfersome and nanostructured lipid carrier gels loaded with *Curcuma longa* and *Glycyrrhiza glabra* (TFS-CGE and NLC-CGE gels) resulted in significant improvements in multiple skin aging parameters. Histological and immunohistochemical analyses revealed reduced epidermal thickness, increased dermal collagen density, and upregulated expression of collagen types I, II, and III, TGF-β, and elastin. Furthermore, skin elasticity was notably enhanced in treated groups. These therapeutic effects are likely mediated through the suppression of UV-B-induced oxidative stress. The bioactive compounds in the formulations are known antioxidants, which reduce ROS levels, thereby inhibiting the MAPK/AP-1 signaling pathway. As a result, MMP-1 expression is downregulated, preventing collagen degradation. At the same time, restoration of the TGF-β–SMAD signaling pathway supports the transcription of ECM components. This integrated molecular modulation underlies the observed structural recovery and functional improvements in skin integrity, supporting the anti-photoaging efficacy of both nanocarrier systems.

In the present study, UV-B radiation triggered various macroscopic changes, such as erythema and wrinkle formation, as a manifestation of photoaging. These phenotypic alterations are largely attributed to the degradation of collagen, a major structural component of the ECM, which plays a key role in maintaining skin strength and integrity. These findings were further supported by histological observations using immunohistochemical staining, which showed a reduction in the expression of collagen types I, II, and III in the dermis following UV-B exposure. However, topical application of *Curcuma longa* and *Glycyrrhiza glabra* extracts formulated in transfersome (TFS-CGE) and nanostructured lipid carrier (NLC-CGE) gels ameliorated UV-B-induced damage, as indicated by increased collagen expression and improved dermal structure. This suggests that the bioactive compounds within CGE exhibit protective effects against ECM degradation and collagen loss.

The ECM is a complex network of proteins and polysaccharides that provides structural and biochemical support to surrounding cells. Collagen and elastin fibers are among its key constituents, and their degradation is a hallmark of photoaging. Excessive UV-B exposure elevates intracellular ROS, which not only induce direct oxidative damage but also activate signaling cascades that exacerbate ECM breakdown. ROS accumulation stimulates the mitogen-ac-

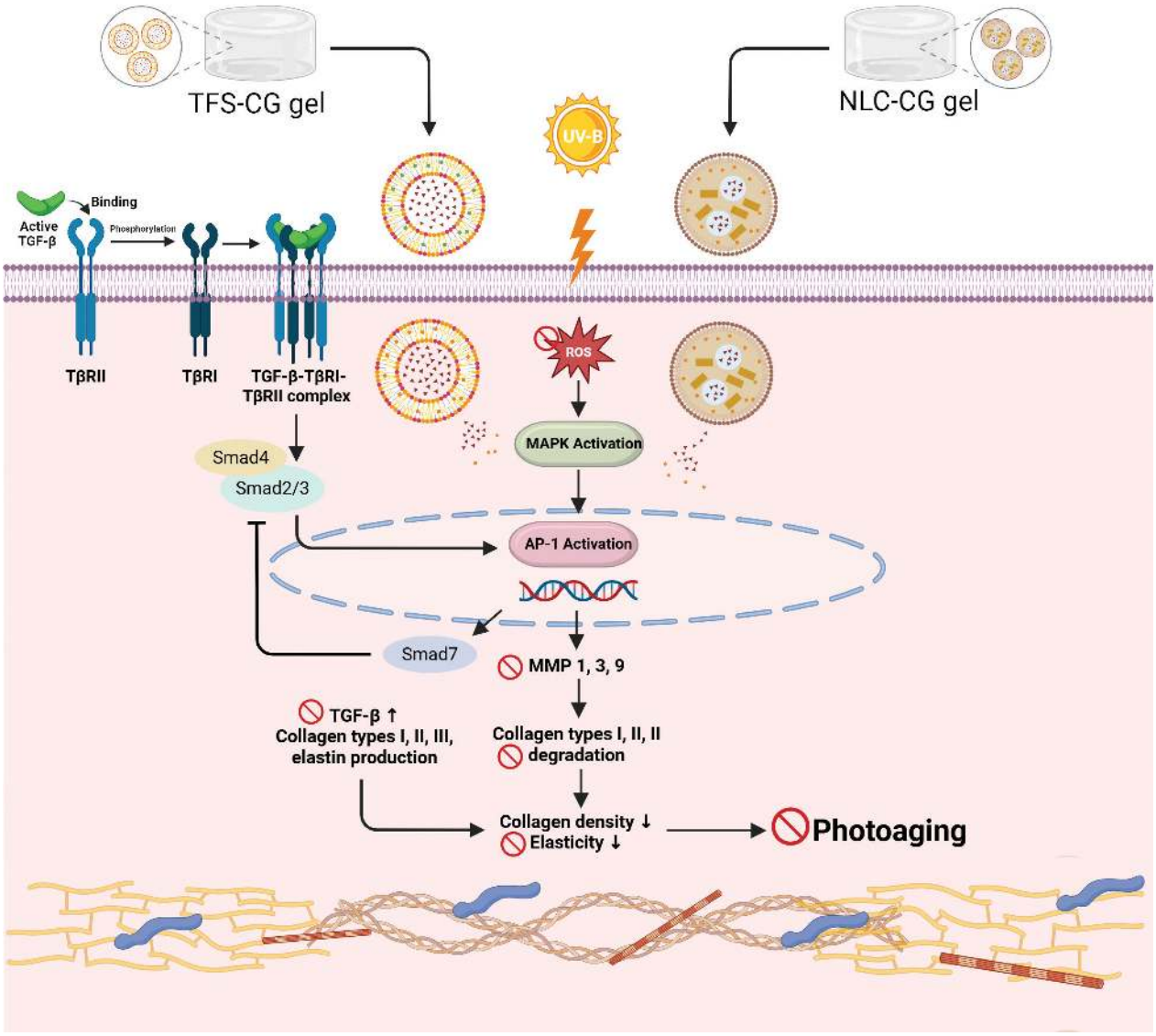


Figure 12. Proposed molecular mechanism of transfersome and NLC containing *Curcuma longa* and *Glycyrrhiza glabra* extract against UV-B-induced skin photoaging. The image was created by BioRender.

tivated protein kinase (MAPK) pathway, ultimately leading to the activation of transcription factors such as AP-1. AP-1, in turn, upregulates matrix metalloproteinases (MMPs), particularly MMP-1 and MMP-3, which are responsible for collagen degradation (Lee et al. 2021). This molecular cascade is strongly implicated in the formation of wrinkles and other features of photoaged skin.

Skin elasticity is highly dependent on the structural integrity and abundance of extracellular matrix components, particularly collagen and elastin. In this study, UV-B exposure significantly impaired skin elasticity, as demonstrated by the prolonged recovery time in the UV-B-irradiated group. This impairment was associated with downregulation of TGF-β, a key cytokine involved in the biosynthesis of collagen and elastin. Concurrently, UV-B irradiation induced overexpression of MMPs, especially MMP-1 and MMP-9, which degrade collagen types I, II, and III and elastin, thereby accelerating extracellular matrix degradation (Jabłońska-Trypuć et al. 2016). In contrast, treatment with TFS-CGE and NLC-CGE gels significantly shortened recovery time, indicating enhanced skin elasticity. This improvement is likely attributed to bioactive compounds in the formulations that upregulated TGF-β expression and suppressed MMP activity, promoting collagen and elastin synthesis and preservation. Comparatively, TFS- and NLC-based gels without extract exhibited longer recovery times, underscoring the therapeutic potential of TFS-CGE and NLC-CGE gels in mitigating photoaging and preserving skin biomechanical properties following UV-induced oxidative stress.

Curcumin, the principal polyphenolic compound in turmeric extract, is a potent antioxidant that exerts its protective effects through multiple mechanisms. It activates the Keap1–NRF2–EpRE signaling pathway, promoting the expression of endogenous antioxidant enzymes such as superoxide dismutase (SOD), heme ox-

ygenase-1 (HO-1), and catalase (CAT), thereby reducing oxidative stress within the skin (Deng et al. 2021). Moreover, curcumin has been shown to inhibit UV-B-induced activation of the p38 MAPK pathway, suppressing the AP-1 transcription factor and thereby downregulating MMP gene expression (Shamsnia et al. 2023). Consistent with these mechanisms, another study demonstrated that curcumin isolated from turmeric extract significantly enhanced type I collagen expression in UV-damaged dermal tissue (Threskeia et al. 2023). In addition, curcumin has also been proven to inhibit the formation of ROS and nuclear factor-κB (NF-κB), thereby reducing the expression of MMP-1, MMP-3, and Smad7 in human dermal fibroblasts (HDFs) (Liu et al. 2018).

Similarly, alkaloid and flavonoid compounds present in licorice (*Glycyrrhiza glabra*) extract have been shown to inhibit MAPK signaling pathways, specifically through the suppression of UV-induced p38 and JNK activation, thereby reducing the expression of MMP-1 and MMP-3 and contributing to the restoration of collagen fiber architecture in dermal tissue exposed to UV-B radiation (Afnan et al. 2016; Farrukh et al. 2015; Li et al. 2021). In addition, glycyrrhizin, the main secondary metabolite, can form a stable complex with MAPK3 through ionic interactions and hydrogen bonding, resulting in inhibition of the MAPK/STAT3/AKT signaling pathway (Zhang et al. 2024). Glycyrrhizic acid in licorice root can also inhibit pro-inflammatory cytokines by suppressing NF-κB through the MAPKs and PI3K/Akt signaling pathways (Liu et al. 2018). The antioxidant properties of licorice alkaloids have been associated with upregulation of NRF2 expression, further enhancing the production of endogenous antioxidants and supporting ECM preservation (Mou et al. 2019).

Both nanocarrier systems—transfersomes and NLC—play essential roles in enhancing dermal delivery, stability, and bioavailability of the bioactive compounds from *Curcuma longa* and *Glycyrrhiza glabra* extracts. Transfersomes, consisting of ultra-deformable phospholipid vesicles, improve transdermal penetration by enabling the vesicles to traverse the narrow intercellular gaps of the stratum corneum while maintaining structural integrity. This mechanism allows effective delivery of actives into deeper skin layers. In other research, transfersome gel was shown to significantly restore collagen structure, reduce MMP-1 expression, and upregulate TGF-β in UVB-exposed skin treated with transfersome gels of *Musa balbisiana* peel (Mayangsari et al. 2024). Meanwhile, NLCs, comprising a mixture of solid and liquid lipids, enhance drug loading efficiency and stability while allowing sustained release of active compounds. The use of NLC loaded with Oroxylin A demonstrated improved skin permeability and superior antioxidant effects in UVB-damaged skin, effectively lowering ROS levels, apoptosis rates, and lipid peroxidation compared with the non-encapsulated form (Zhu et al. 2022). Together, these delivery strategies support the anti-photoaging potential of TFS-CGE and NLC-CGE gels, highlighting the importance of nanocarrier systems in optimizing anti-aging delivery.

Conclusion

Transfersome and NLC systems loaded with *Curcuma longa* and *Glycyrrhiza glabra* extracts were successfully formulated and characterized, demonstrating favorable nanoscale properties. Both formulations showed strong antioxidant and anti-collagenase activity *in vitro*. When applied as gels *in vivo*, they improved skin elasticity, reduced epidermal thickness, and modulated key aging biomarkers. These findings highlight their potential as effective natural anti-aging agents in nanocarrier-based cosmetic applications.

Additional information

Conflict of interest

The authors have declared that no competing interests exist.

Ethical statements

The authors declared that no clinical trials were used in the present study.

The authors declared that no experiments on humans or human tissues were performed for the present study.

The authors declared that no informed consent was obtained from the humans, donors or donors' representatives participating in the study.

Experiments on animals: All animal experimental procedures and protocols were approved by the Ethics Committee, Faculty of Medicine, Brawijaya University, Indonesia (Number 155/EC/KEPK/06/2024)

The authors declared that no commercially available immortalised human and animal cell lines were used in the present study.

Use of AI

This study used artificial intelligence (AI) tools for manuscript writing support. Specifically, ChatGPT was employed for language refinement and technical writing assistance. We confirm that all AI-assisted processes were critically reviewed by the authors to ensure the integrity and reliability of the results. The final decisions and interpretations presented in this article were solely made by the authors.

Funding

The authors acknowledge financial support from the Faculty of Medicine, Universitas Brawijaya, with grant number 3237/UN10.F08/PN/2024.

Author contributions

Oktavia Rahayu Adianingsih: Conceptualization, Methodology, Writing – Review & Editing, Supervision; Salma Latifani, Annisa Nur Fitriani: Investigation, Writing – Original Draft; Anistasya Dwitama Wardani: Investigation, Writing – Original Draft; Iffah Qurrotuain: Formal analysis, Investigation, Writing – Original Draft; Rachmad Tri Wahyudi: Data curation, Investigation, Writing – Original Draft; Azizah Maharani Putri Dewi: Formal analysis, Investigation, Writing – Original Draft; Jessica Aurellia Wahyu Dhinata: Investigation, Writing – Original Draft;

Gloria Angelica Rumabutar: Investigation, Writing – Original Draft; Oktavia Eka Puspita: Methodology, Writing – Review & Editing, Supervision; Bachtiar Rifai Pratita Ihsan: Methodology, Writing – Review & Editing, Supervision; Wibi Riawan: Writing – Review & Editing, Supervision; Adeltrudis Adelsa Danimayostu: Writing – Review & Editing, Supervision; Valentina Yurina: Writing – Review & Editing, Supervision

Author ORCIDs

Oktavia Rahayu Adianingsih https://orcid.org/0000-0002-7598-0897
Salma Latifani https://orcid.org/0009-0006-6644-5274
Annisa Nur Fitriani https://orcid.org/0009-0002-5565-5728
Anistasya Dwitama Wardani https://orcid.org/0009-0001-7713-503X
Iffah Qurrotuain https://orcid.org/0009-0003-4132-5717
Rachmad Tri Wahyudi https://orcid.org/0009-0002-4413-859X
Azizah Maharani Putri Dewi https://orcid.org/0009-0003-1061-1294
Jessica Aurellia Wahyu Dhinata https://orcid.org/0009-0007-7401-1174
Gloria Angelica Rumabutar https://orcid.org/0009-0000-5108-453X
Oktavia Eka Puspita https://orcid.org/0000-0001-6107-1089
Bachtiar Rifai Pratita Ihsan https://orcid.org/0000-0001-9183-1237
Wibi Riawan https://orcid.org/0000-0001-5822-3846
Adeltrudis Adelsa Danimayostu https://orcid.org/0000-0003-4642-5330
Valentina Yurina https://orcid.org/0000-0003-4319-942X

Data availability

All of the data that support the findings of this study are available in the main text.

References

Adianingsih OR, Fajrin FF, Johan CK (2024) Exploring the mechanism of *Glycyrrhiza glabra* and *Curcuma domestica* against skin photoaging based on network pharmacology. Indonesian Journal of Biotechnology 29: 98–110. https://doi.org/10.22146/ijbiotech.93332

Adianingsih OR, Yurina V, Puspita OE, Widasmara D, Hariyono D, Dhinata JAW (2024) Antioxidant activity of facial wash, moisturizer, and serum containing *Andrographis paniculata* extract, *Syzygium aromaticum* oil, and *Pogostemon cablin* oil. Tropical Journal of Natural Product Research 8: 7575–7579. https://doi.org/10.26538/tjnpr/v8i6.38

Afnan Q, Kaiser PJ, Rafiq RA, Nazir LA, Bhushan S, Bhardwaj SC, Sandhir R, Tasduq SA (2016) Glycyrrhizic acid prevents ultraviolet-B-induced photodamage: A role for mitogen-activated protein kinases, nuclear factor kappa B and mitochondrial apoptotic pathway. Experimental Dermatology 25: 440–446. https://doi.org/10.1111/exd.12964

Ahad A, Al-Saleh AA, Al-Mohizea AM, Al-Jenoobi FI, Raish M, Yassin AEB, Alam MA (2018) Formulation and characterization of phospholipon 90 G and tween 80 based transfersomes for transdermal delivery of eprosartan mesylate. Pharmaceutical Development and Technology 23: 787–793. https://doi.org/10.1080/10837450.2017.1330345

Ahalwat S, Bhatt DC (2022) Development of novel lipid matrix for improved sustained release effect of a hydrophilic drug via response surface methodology. Journal of Drug Delivery Science and Technology 67. https://doi.org/10.1016/j.jddst.2021.102993

Al Shuwaili AH, Rasool BKA, Abdulrasool AA (2016) Optimization of elastic transfersomes formulations for transdermal delivery of pentoxifylline. European Journal of Pharmaceutics and Biopharmaceutics 102: 101–114. https://doi.org/10.1016/j.ejpb.2016.02.013

Altay Benetti A, Tarbox T, Benetti C (2023) Current insights into the formulation and delivery of therapeutic and cosmeceutical agents for aging skin. Cosmetics 10: 54. https://doi.org/10.3390/cosmetics10020054

AOAC (2023) AOAC Official Methods of Analysis.

Asensio-Regalado C, Alonso-Salces RM, Gallo B, Berrueta LA, Era B, Pintus F, Caddeo C (2022) Tempranillo grape extract in transfersomes: a nanoproduct with antioxidant activity. Nanomaterials 12: 746. https://doi.org/10.3390/nano12050746

Assali M, Zaid AN (2022) Features, applications, and sustainability of lipid nanoparticles in cosmeceuticals. Saudi Pharmaceutical Journal 30: 53–65. https://doi.org/10.1016/j.jsps.2021.12.018

Avadhani KS, Manikkath J, Tiwari M, Chandrasekhar M, Godavarthi A, Vidya SM, Hariharapura RC, Kalthur G, Udupa N, Mutalik S (2017) Skin delivery of epigallocatechin-3-gallate (EGCG) and hyaluronic acid loaded nano-transfersomes for antioxidant and anti-aging effects in UV radiation induced skin damage. Drug Delivery 24: 61–74. https://doi.org/10.1080/10717544.2016.1228718

Ayunin Q, Miatmoko A, Soeratri W, Erawati T, Susanto J, Legowo D (2022) Improving the anti-ageing activity of coenzyme Q10 through protransfersome-loaded emulgel. Scientific Reports 12: 906. https://doi.org/10.1038/s41598-021-04708-4

Benameur T, Soleti R, Panaro MA, La Torre ME, Monda V, Messina G, Porro C (2021) Curcumin as prospective anti-aging natural compound: focus on brain. Molecules 26: 4794. https://doi.org/10.3390/molecules26164794

Bnyan R, Khan I, Ehtezazi T, Saleem I, Gordon S, O'neill F, Robert M (2019) Formulation and optimisation of novel transfersomes for sustained release of local anaesthetic. Journal of Pharmacy and Pharmacology 71: 1508–1519. https://doi.org/10.1111/jphp.13149

Cerulli A, Masullo M, Montoro P, Piacente S (2022) Licorice (*Glycyrrhiza glabra*, *G. uralensis*, and *G. inflata*) and their constituents as active cosmeceutical ingredients. Cosmetics 9: 7. https://doi.org/10.3390/cosmetics9010007

Chabru AS, Salve PS, Ghumare GD, Dhamak RS, Tiwari DR, Waghmare DS (2024) Comparative pharmacokinetic studies of transferosomes loaded gel and pressure sensitive adhesive based patch formulation for transdermal delivery of benztropine mesylate. Journal of Drug Delivery Science and Technology 92: 105287. https://doi.org/10.1016/j.jddst.2023.105287

Chaiyana W, Charoensup W, Sriyab S, Punyoyai C, Neimkhum W (2021) Herbal extracts as potential antioxidant, anti-aging, anti-inflammatory, and whitening cosmeceutical ingredients. Chemistry & Biodiversity 18: e2100245. https://doi.org/10.1002/cbdv.202100245

Chauhan I, Yasir M, Verma M, Singh AP (2020) Nanostructured lipid carriers: a groundbreaking approach for transdermal drug delivery. Advanced Pharmaceutical Bulletin 10(2): 150–165. https://doi.org/10.34172/apb.2020.021

Chawla A, Lobacz A, Tarapata J, Zulewska J (2021) UV light application as a mean for disinfection applied in the dairy industry. Applied Sciences 11: 7285. https://doi.org/10.3390/app11167285

Costa EF, Magalhães WV, Di Stasi LC (2022) Recent advances in herbal-derived products with skin anti-aging properties and cosmetic applications. Molecules 27: 7518. https://doi.org/10.3390/molecules27217518

Das B, Nayak AK, Mallick S (2023) Thyme oil–containing fluconazole-loaded transferosomal bigel for transdermal delivery. AAPS PharmSciTech 24: 240. https://doi.org/10.1208/s12249-023-02698-2

Deng H, Wan M, Li H, Chen Q, Li R, Liang B, Zhu H (2021) Curcumin protection against ultraviolet-induced photo-damage in Hacat cells by regulating nuclear factor erythroid 2-related factor 2. Bioengineered 12: 9993–10006. https://doi.org/10.1080/21655979.2021.1994720

Deng Z, Fan T, Xiao C, Tian H, Zheng Y, Li C, He J (2024) TGF-β signaling in health, disease, and therapeutics. Signal Transduction and Targeted Therapy 9: 61. https://doi.org/10.1038/s41392-024-01764-w

Dhavale RP, Nadaf SJ, Bhatia MS (2021) Quantitative structure property relationship assisted development of fluocinolone acetonide loaded transfersomes for targeted delivery. Journal of Drug Delivery Science and Technology 65: 102758. https://doi.org/10.1016/j.jddst.2021.102758

Dudhipala N, Mohammed RP, Youssef AAA, Banala N (2020) Effect of lipid and edge activator concentration on development of aceclofenac-loaded transfersomes gel for transdermal application: in vitro and ex vivo skin permeation. Drug Development and Industrial Pharmacy 1334–1344. https://doi.org/10.1080/03639045.2020.1788069

El Zaafarany GM, Awad GAS, Holayel SM, Mortada ND (2010) Role of edge activators and surface charge in developing ultradeformable vesicles with enhanced skin delivery. International Journal of Pharmaceutics 397: 164–172. https://doi.org/10.1016/j.ijpharm.2010.06.034

El-Gizawy SA, Nouh A, Saber S, Kira AY (2020) Deferoxamine-loaded transfersomes accelerates healing of pressure ulcers in streptozotocin-induced diabetic rats. Journal of Drug Delivery Science and Technology 58: 101732. https://doi.org/10.1016/j.jddst.2020.101732

Farrukh MR, Nissar UA, Kaiser PJ, Afnan Q, Sharma PR, Bhushan S, Tasduq SA (2015) Glycyrrhizic acid (GA) inhibits reactive oxygen species mediated photodamage by blocking ER stress and MAPK pathway in UV-B irradiated human skin fibroblasts. Journal of Photochemistry and Photobiology B: Biology 148: 351–357. https://doi.org/10.1016/j.jphotobiol.2015.05.003

Fernández-García R, Lalatsa A, Statts L, Bolás-Fernández F, Ballesteros MP, Serrano DR (2020) Transferosomes as nanocarriers for drugs across the skin: quality by design from lab to industrial scale. International Journal of Pharmaceutics. 573: 118817. https://doi.org/10.1016/j.ijpharm.2019.118817

Garg V, Singh H, Bhatia A, Raza K, Singh SK, Singh B, Beg S (2017) Systematic development of transethosomal gel system of piroxicam: formulation optimization in vitro evaluation and ex vivo assessment. AAPS PharmSciTech 18: 58–71. https://doi.org/10.1208/s12249-016-0489-z

Ghasemiyeh P, Mohammadi-Samani S (2018) Solid lipid nanoparticles and nanostructured lipid carriers as novel drug delivery systems: applications advantages and disadvantages. Research in Pharmaceutical Sciences 13: 288–303. https://doi.org/10.4103/1735-5362.235156

Goindi S, Kumar G, Kumar N, Kaur A (2013) Development of novel elastic vesicle-based topical formulation of cetirizine dihydrochloride for treatment of atopic dermatitis. AAPS PharmSciTech 14: 1284–1293. https://doi.org/10.1208/s12249-013-0017-3

Gomaa E, Fathi HA, Eissa NG, Elsabahy M (2022) Methods for preparation of nanostructured lipid carriers. Methods 199: 3–8. https://doi.org/10.1016/j.ymeth.2021.05.003

Gupta A, Aggarwal G, Singla S, Arora R (2012) Transfersomes: a novel vesicular carrier for enhanced transdermal delivery of sertraline: development characterization and performance evaluation. Scientia Pharmaceutica 80: 1061–1080. https://doi.org/10.3797/scipharm.1208-02

Haider M, Abdin SM, Kamal L, Orive G (2020) Nanostructured lipid carriers for delivery of chemotherapeutics: a review. Pharmaceutics 12: 288. https://doi.org/10.3390/pharmaceutics12030288

Harmita H, Iskandarsyah I, Afifah SF (2020) Effect of transfersome formulation on the stability and antioxidant activity of n-acetylcysteine in anti-aging cream. International Journal of Applied Pharmaceutics 12: 156–162. https://doi.org/10.22159/ijap.2020.v12s1.FF034

Indian Pharmacopoeia Commission (2021) Guidance Document Validation of Analytical Methods Indian Pharmacopoeia Commission.

Jabłońska-Trypuć A, Matejczyk M, Rosochacki S (2016) Matrix metalloproteinases (MMPs) the main extracellular matrix (ECM) enzymes in collagen degradation as a target for anticancer drugs. Journal of Enzyme Inhibition and Medicinal Chemistry 31(S1): 177–183. https://doi.org/10.3109/14756366.2016.1161620

Kaul S, Gulati N, Verma D, Mukherjee S, Nagaich U (2018) Role of nanotechnology in cosmeceuticals: a review of recent advances. Journal of Pharmaceutics 2018: 3420204. https://doi.org/10.1155/2018/3420204

Khan I, Needham R, Yousaf S, Houacine C, Islam Y, Bnyan R, Sadozai SK, Elrayess MA, Elhissi A (2021) Impact of phospholipids surfactants and cholesterol selection on the performance of transfersomes vesicles using medical nebulizers for pulmonary drug delivery. Journal of Drug Delivery Science and Technology 66: 102822. https://doi.org/10.1016/j.jddst.2021.102822

Khan MA, Pandit J, Sultana Y, Sultana S, Ali A, Aqil M, Chauhan M (2015) Novel carbopol-based transfersomal gel of 5-fluorouracil for skin cancer treatment: in vitro characterization and in vivo study. Drug Delivery 22(6): 795–802. https://doi.org/10.3109/10717544.2014.902146

Khan MI, Yaqoob S, Madni A, Akhtar MF, Sohail MF, Saleem A, Tahir N, Khan K ur R, Qureshi OS (2022) Development and in vitro / ex vivo evaluation of lecithin-based deformable transfersomes and transfersome-based gels for combined dermal delivery of meloxicam and dexamethasone. BioMed Research International 2022: 8170318. https://doi.org/10.1155/2022/8170318

Khatoon K, Rizwanullah M, Amin S, Mir SR, Akhter S (2019) Cilnidipine loaded transfersomes for transdermal application: Formulation optimization in-vitro and in-vivo study. Journal of Drug Delivery Science and Technology 54: 101303. https://doi.org/10.1016/j.jddst.2019.101303

Lee H, Hong Y, Kim M (2021) Structural and functional changes and possible molecular mechanisms in aged skin. International Journal of Molecular Sciences 22: 12489. https://doi.org/10.3390/ijms222212489

Li Y, Xia C, Yao G, Zhang X, Zhao J, Gao X, Yong J, Wang H (2021) Protective effects of liquiritin on UVB-induced skin damage in SD rats. International Immunopharmacology 97: 107614. https://doi.org/10.1016/j.intimp.2021.107614

Lin CL, Li YL, Chen YW, Kuo CH, Tu TY, Liu YF, Tsai JC, Shyong YJ (2024) Amphiphilic NLC-gel formulation loaded with Sebacoyl dinalbuphine ester and nalbuphine for localized postoperative pain management. International Journal of Pharmaceutics 659: 124295. https://doi.org/10.1016/j.ijpharm.2024.124295

Liu X, Zhang R, Shi H, Li X, Li Y, Taha A, Xu C (2018) Protective effect of curcumin against ultraviolet A irradiation-induced photoaging in human dermal fibroblasts. Molecular Medicine Reports 17: 7227–7237. https://doi.org/10.3892/mmr.2018.8791

Manosroi A, Chutoprapat R, Abe M, Manosroi W, Manosroi J (2012) Anti-aging efficacy of topical formulations containing niosomes en-

trapped with rice bran bioactive compounds. Pharmaceutical Biology 50: 208–224. https://doi.org/10.3109/13880209.2011.596206

Matei AM, Caruntu C, Tampa M, Georgescu SR, Matei C, Constantin MM, Constantin TV, Calina D, Ciubotaru DA, Badarau IA, Scheau C, Caruntu A (2021) Applications of nanosized-lipid-based drug delivery systems in wound care. Applied Sciences 11: 4915. https://doi.org/10.3390/app11114915

Mayangsari E, Mustika A, Nurdiana N, Samad N (2024) Ameliorative effect of transfersome gel of kepok banana peel extract (*Musa balbisiana*) against photoaging in Wistar rat skin. Open Veterinary Journal 14: 1990. https://doi.org/10.5455/ovj.2024.v14.i8.28

Minister of Health of the Republic of Indonesia (2017) Indonesian Herbal Pharmacopoeia II Ed. Jakarta.

Miyazawa K, Miyazono K (2017) Regulation of TGF-β family signaling by inhibitory Smads. Cold Spring Harbor Perspectives in Biology 9: a022095. https://doi.org/10.1101/cshperspect.a022095

Mou K, Pan W, Han D, Wen X, Cao F, Miao Y, Li P (2019) Glycyrrhizin protects human melanocytes from H_2O_2-induced oxidative damage via the Nrf2 dependent induction of HO-1. International Journal of Molecular Medicine 44: 253–261. https://doi.org/10.3892/ijmm.2019.4200

Németh Z, Pallagi E, Dobó DG, Kozma G, Kónya Z, Csóka I (2021) An updated risk assessment as part of the QbD-based liposome design and development. Pharmaceutics 13(7): 1071. https://doi.org/10.3390/pharmaceutics13071071

Pardeike J, Schwabe K, Müller RH (2010) Influence of nanostructured lipid carriers (NLC) on the physical properties of the Cutanova Nanorepair Q10 cream and the in vivo skin hydration effect. International Journal of Pharmaceutics 396: 166–173. https://doi.org/10.1016/j.ijpharm.2010.06.007

Quan T, He T, Voorhees JJ, Fisher GJ (2005) Ultraviolet irradiation induces Smad7 via induction of transcription factor AP-1 in human skin fibroblasts. Journal of Biological Chemistry 280: 8079–8085. https://doi.org/10.1074/jbc.M409647200

Quan T, He T, Voorhees JJ, Fisher GJ (2001) Ultraviolet irradiation blocks cellular responses to transforming growth factor-β by down-regulating its type-ii receptor and inducing Smad7. Journal of Biological Chemistry 276: 26349–26356. https://doi.org/10.1074/jbc.M010835200

Reddy PS, Jagarlapudi VSK, Sekharan CB (2016) Determination of edoxaban in bulk and in tablet dosage form by stability indicating high-performance liquid chromatography. Pharmaceutical Sciences 22: 35–41. https://doi.org/10.15171/PS.2016.07

Saraf S, Jeswani G, Kaur CD, Saraf S (2011) Development of novel cosmetic cream with *Curcuma longa* extract loaded transfersomes for anti-wrinkle effect. African Journal of Pharmacy and Pharmacology 5 (8): 1054–1062. https://doi.org/10.5897/AJPP11.226

Sguizzato M, Esposito E, Cortesi R (2021) Lipid□based nanosystems as a tool to overcome skin barrier. International Journal of Molecular Sciences 22: 8319. https://doi.org/10.3390/ijms22158319

Shamsnia HS, Roustaei M, Ahmadvand D, Butler A, Amirlou D, Soltani S, Momtaz S, Jamialahmadi T, Abdolghaffari AH, Sahebkar A (2023) Impact of curcumin on p38 MAPK: therapeutic implications. Inflammopharmacology 31: 2201–2212. https://doi.org/10.1007/s10787-023-01265-2

Shimojo AAM, Fernandes ARV, Ferreira NRE, Sanchez-Lopez E, Santana MHA, Souto EB (2019) Evaluation of the influence of process parameters on the properties of resveratrol-loaded NLC using 22 full factorial design. Antioxidants 8: 272. https://doi.org/10.3390/antiox8080272

Subramaniam B, Siddik ZH, Nagoor NH (2020) Optimization of nanostructured lipid carriers: understanding the types designs and parameters in the process of formulations. Journal of Nanoparticle Research 22: 141. https://doi.org/10.1007/s11051-020-04848-0

Surini S, Sarah, Djajadisastra J (2018) Formulation and in vitro penetration study of transfersomes gel containing gotu kola leaves extract (*Centella asiatica* L. Urban). Journal of Young Pharmacists 10(1): 27–31. https://doi.org/10.5530/jyp.2018.10.8

Taymouri S, Hajhashemi V, Tabbakhian M, Torkashvand M (2021) Preparation and evaluation of imatinib loaded transfersomal gel for the treatment of rheumatoid arthritis. Iranian Journal of Pharmaceutical Research 20(4): 33–46. https://doi.org/10.22037/ijpr.2021.115481.15394

Threskeia A, Sandhika W, Rahayu RP (2023) Effect of turmeric (*Curcuma longa*) extract administration on tumor necrosis factor alpha and type 1 collagen expression in UVB-light radiated BALB/c mice. Journal of Applied Pharmaceutical Science 13(5): 121–125. https://doi.org/10.7324/JAPS.2023.19358

Tsukahara K, Moriwaki S, Hotta M, Fujimura T, Sugiyama-Nakagiri Y, Sugawara S, Kitahara T, Takema Y (2005) The effect of sunscreen on skin elastase activity induced by ultraviolet-A irradiation. Biological and Pharmaceutical Bulletin 28 (12): 2302–2307. https://doi.org/10.1248/bpb.28.2302

United States Pharmacopoeia 36 (2017) Analytical Performance Characteristics.

Vardhini NM, Punia J, Jat S, Pawar SD, Devi N, Radhakrishnanand P, Murty US, Saini A, Sethi KK, Kumar P (2023) Purification and characterization of pure curcumin desmethoxycurcumin and bisdemethoxycurcumin from North-East India Lakadong turmeric (*Curcuma longa*). Journal of Chromatography A 1708: 464358. https://doi.org/10.1016/j.chroma.2023.464358

Waghule T, Gorantla S, Rapalli VK, Shah P, Dubey SK, Saha RN, Singhvi G (2020) Emerging trends in topical delivery of curcumin through lipid nanocarriers: effectiveness in skin disorders. AAPS PharmSciTech 21: 284. https://doi.org/10.1208/s12249-020-01831-9

Wei M, He X, Liu N, Deng H (2024) Role of reactive oxygen species in ultraviolet-induced photodamage of the skin. Cell Division 19:1. https://doi.org/10.1186/s13008-024-00107-z

Weiss J, Decker EA, McClements DJ, Kristbergsson K, Helgason T, Awad T (2008) Solid lipid nanoparticles as delivery systems for bioactive food components. Food Biophysics 3: 146–154. https://doi.org/10.1007/s11483-008-9065-8

World Health Organization (2002) WHO Monograph on Selected Medicinal Plants Volume I. World Health Organization.

Zhang R, Asikaer A, Chen Q, Wang F, Lan J, Liu Y, Hu L, Zhao H, Duan H (2024) Network pharmacology and in vitro experimental verification unveil glycyrrhizin from *Glycyrrhiza glabra* alleviates acute pancreatitis via modulation of MAPK and STAT3 signaling pathways. BMC Complement Medicine and Therapies 24: 58. https://doi.org/10.1186/s12906-024-04372-x

Zheng Y, Pan C, Zhang Z, Luo W, Liang X, Shi Y, Liang L, Zheng X, Zhang L, Du Z (2020) Antiaging effect of *Curcuma longa* L. essential oil on ultraviolet-irradiated skin. Microchemical Journal 154: 104608. https://doi.org/10.1016/j.microc.2020.104608

Zhu S, Zhao Z, Qin W, Liu T, Yang Y, Wang Z, Ma H, Wang X, Qi D, Guo P, Pi JX, Tian BC, Zhang H, Li N (2022) The nanostructured lipid carrier gel of oroxylin A reduced UV-induced skin oxidative stress damage. Colloids and Surface B: Biointerfaces 216: 112578. https://doi.org/10.1016/j.colsurfb.2022.112578